2024 HIRA IMANULLAH SU92-MSCHW-F22-040 FOS

Synthesis Of High Entropy Aerogels for Photocatalytic Carbondioxide Reduction

SUPERIOR UNIVERSITY

Thesis Submitted to

The Superior University Lahore

In Partial Fulfillment of the

Requirement for the Degree of

M.Phil. Chemistry

By

HIRA IMANULLAH

SU92-MSCHW-F22-040

Session: 2022-2024

Faculty of Sciences

Synthesis Of High Entropy Aerogels for Photocatalytic Carbondioxide Reduction

SUPERIOR UNIVERSITY

Thesis Submitted to

The Superior University Lahore

In Partial Fulfillment of the

Requirement for the Degree of

M.Phil. Chemistry

By

HIRA IMANULLAH

SU92-MSCHW-F22-040

Session: 2022-2024

Faculty of Sciences

Author's Declaration

I hereby state that my M.Phil. thesis titled **"Synthesis of high entropy aerogels for photocatalytic carbondioxide reduction"** is my work and has not been submitted previously by me for taking any degree from this University,

The Superior University, Lahore

or anywhere else in the country/world.

At any time if my statement is found to be incorrect even after my graduation, the university has the right to withdraw my M.Phil. degree.

Name of Student: Hira Imanullah

Date: _____

Plagiarism Undertaking

I solemnly declare that research work presented in the thesis titled **"Synthesis of high entropy aerogels for photocatalytic carbondioxide reduction"** is solely my research work with no significant contribution from any other person. Small contribution/help wherever taken has been duly acknowledged and that complete thesis has been written by me.

I understand the zero-tolerance policy of the HEC and University,

The Superior University, Lahore

towards plagiarism. Therefore, I as author of the above-titled thesis declare that no portion of my thesis has been plagiarized and any material used as a reference is properly referred/cited. I undertake that if I am found guilty of any formal plagiarism in the above-titled thesis, even after awarding of M.Phil. degree, the University reserves the rights to withdraw/revoke my M.Phil. degree and that HEC and the University have the right to publish my name on the HEC/University website on which names of students are placed who submitted a plagiarized thesis.

Student/Author Signature: _____

Name: Hira Imanullah

Research Completion Certificate

This is to certify that the thesis entitled **"Synthesis of high entropy aerogel for photocatalytic carbondioxide reduction"** submitted by **"Hira Imanullah"** has been accepted towards the partial fulfillment of the requirement for M.Phil. **"Chemistry"**. The quality of the work contained in this thesis is adequate for the award of degree.

Supervisor Name: Dr. Fizza Naseem

Designation: Assistant Professor

Signature: _____

Certificate of Approval

This is to certify that the research work presented in this thesis, titled **"Synthesis of high entropy aerogels for photocatalytic carbondioxide reduction"** was conducted by **"Hira Imanullah"** under the supervision of **"Dr. Fizza Naseem"**

No part of this thesis has been submitted anywhere else for any other degree. This thesis is submitted to the Faculty of Sciences, The Superior University, Lahore in partial fulfillment of the requirements for the degree of Master of Science/Master of Philosophy in the field of "**M.Phil. Chemistry"** in Faculty of Sciences at The Superior University, Lahore.

Student Name: Hira Imanullah Signature:_____

Examination Committee:

Session Chair: Signature:_____

a) External Examiner: Signature:_____

b) Internal Examiner: Signature:_____

c) Supervisor Name: Signature:_____

d) Name of HOD: Prof. Dr. Uqba Mehmood Signature:_____

e) Name of Dean: Prof. Dr. Mohammad Naveed Babur Signature:_____

f) Controller Examination: Dr. Muhammad Haris Signature:_____

Dedication

With deepest gratitude and heartfelt admiration, I dedicate this thesis to those who have been my pillars of strength and inspiration throughout this journey.

To my beloved parents, whose unwavering support, unconditional love, and boundless faith in my abilities have been the guiding light in my life. Your sacrifices, encouragement, and belief in me have made this achievement possible.

To Dr. Fizza Naseem, your wisdom and guidance have profoundly shaped my intellectual and personal growth. You have been a beacon of inspiration and a reminder of the transformative power of education.

To all dreamers, seekers, and scholars who strive for truth and understanding, may this work stand as a humble tribute to the relentless pursuit of knowledge and the enduring spirit of curiosity.

To all who have taught me the value of resilience, humility, and kindness, this thesis is as much yours as it is mine.

Acknowledgments

In the name of Allah, the most Gracious, the most Merciful.

I am extremely thankful to Almighty ‘Allah’, Who is the entire source of knowledge and wisdom endowed to mankind, for providing me with the acumen and vision to complete this endeavor.

I would like to express my profound gratitude to my supervisor, Dr. Fizza Naseem, for her wise counsel and encouraging attitude towards this study. I am extremely grateful to her for immensely facilitating me during my study period by ensuring the provision of favorable circumstances and a conducive environment. This project would not have been possible without her support and expert guidance.

In the end, I would like to extend my deepest gratitude to my family members. Without their encouragement, I would not have been able to complete this endeavor

Hira Imanullah

Table of Contents **Page**

Author's Declaration……I

Plagiarism Undertaking……...II

Research Completion Certificate……III

Certificate of Approval…..IV

DEDICATION…….V

ACKNOWLEDGEMENTS……. VI

TABLE OF CONTENTS…. VII

LIST OF TABLES……. XII

LIST OF FIGURES…….XIII

LIST OF ABBREVATIONS……. XIV

ABSTRACT…….XV

CHAPTER 1…….01

INTRODUCTION …….01

1.1 Porous Materials…….01

1.2 Uses of permeable substances…….…02

1.1.1 Catalytic activity……..…02

1.1.2 Isolation and retention…… 03

1.1.3 Energy……...…… 03

1.1.4 Construction……...…… 04

1.1.5 Drug……...…… 04

1.1.6 Bioreactors……...……05

1.2 Aerogel…….....05

1.2.1 Hydrogel……...…… 05

1.2.2 Cryogel……...……06

1.2.3 Supercritical CO_2…….... 06

1.3 Discovery of aerogel……..... 06

1.4 The properties of aerogels…….....…07

1.5 Applications of Aerogels……..... 08

1.5.1 Insulation……...……08

1.5.2 Storage…….. ……08

1.5.3 Environment……...……09

1.5.4 Catalysis……...……09

1.5.5 Energy……...……09

1.5.6 Hypervelocity particles capture…… 09

1.5.7 Porous support……...…10

1.7 Supercritical Carbon Dioxide……...10

1.8 High Entropy Aerogel…….....10

AIMS AND OBJECTIVES…….....12

CHAPTER 2 …….....13

LITERATURE REVIEW…….....13

1.1 Introduction To HEAAS…….....13

2.2 Synthesis Methods For HEAAS…….....13

2.2.1 Chelating Co-Reduction Strategy……13

2.2.2 Freeze-Thaw Method……...13

2.2.3 In-Situ Carbothermal Reduction ……13

2.3.4 Supercritical Carbon dioxide Synthesis……14

2.3 Hybrid Aerogels and CO_2 Capture…….....14

2.4 Characterization and Properties……...…14

2.4.1 Microstructure and Morphology…… 14

2.4.2 Surface area and Porosity Analysis…… 14

2.4.3 Thermal and Mechanical Properties…… 15

2.4.4 Performance of High Entropy Aerogel……15

2.5 Characterization Methods for High Entropy Aerogels……15

2.5.1 Methods of Microscopy…….15

2.5.2 X-ray Diffraction Analysis……15

2.6 High Entropy Materials (HEMs) and Environmental Applications……15

2.7 High-Entropy Alloys (HEAs) and Their Properties……16

2.7.1 Computational Techniques and HEA Catalyst……16

2.7.2 Specific Examples and Performance of HEAAs……16

2.8 Research Focus and Developments in Aerogel Science…… 17

2.9 A Novel Material for Thermal Barrier Coatings with Enhanced Thermal Insulation and Stability…….....……17

2.10 High Entropy Oxides (HEOs) as Advanced Electrocatalysts for Water Oxidation Reactions…….....……18

2.11Enhanced CO_2 Capture Using K_2CO_3-Impregnated Carbon Aerogel Nanocomposites Under Moist Conditions…….....19

2.12 Enhanced CO_2 Adsorption Using Nitrogen-Doped Carbon Aerogels Synthesized with Urea…….....……20

2.13 High Entropy Alloys for Enhanced Oxygen Evolution Reaction (OER) Activity and Stability in Water Electrolysis…….....21

2.14 Future Directions in HEAAs and Aerogels…….22

CHAPTER 3 …….....24

METHODOLOGY…….....24

3.1 Materials…….....24

3.2 Apparatus…….....24

3.3 Synthesis Of HEAG…….....24

3.3.1 Synthesis of CuO-HEAG@rGO…… 25

3.4 Photocatalytic CO_2 Reduction…….....25

CHAPTER 4…….....27

RESULTS …….....27

4.1 UV-Vis Spectroscopy Analysis …….....27

4.2 FT-IR Spectroscopy Analysis…….....……29

4.3 PL Spectroscopy Analysis…….....……30

4.4 SEM Analysis …….....……31

4.5 XPS Analysis…….....……32

4.6 XRD Analysis…….....……34

4.7 GC Analysis..... 36

4.8 Photocatalytic CO_2 Reduction into Methanol…….……38

CHAPTER 5 …….....42

DISCUSSION…….....42

CHAPTER 6…….....44

CONCLUSION …….....44

REFERENCES….....45

List of Tables **Description** **Page**

Table 1 GCFID Signals Data.....38
Table 2 Comparison of Yield.....39

List of Figures **Description** **Page**

Figure 1: Diagram of Aerogels before and after calcination.....25
Figure 2: Lab-build Photocatalytic reaction chamber.....26
Figure 3: UV-vis absorption spectrum..... 28
Figure 4: The FTIR spectrum reveals several important vibrational modes……..……29
Figure 5: PL Spectrum.....31
Figure 6: SEM images of HEA gel nanocomposites …….....32
Figure 7: XPS Graphs a, b, c, d, e, f, g shows elemental composition and oxidation states of Cu, Se, O, C, Mo, Co, W ……33,34
Figure 8: XRD pattern showing the characteristic diffraction peaks of the analyzed samples.35
Figure 9: GC (a) methanol standard chromatogram data vs (b) HEAG methanol chromatogram And (c) CuO-HEAG@rGO methanol chromatogram ……...……37
Figure 10: Methanol yield of HEAG and HEAG@CuO@rGO …….. 40

List of Abbreviations

HEAG	High entropy aerogel gel
CuO	Copper oxide
Se	Selenium
GO	Graphene oxide
rGO	Reduced graphene oxide

ABSTRACT

Aerogel is a thin, highly porous substance that is made from gels in which the liquid component is swapped out for a gas. It is among the lightest solid materials known to exist because of its incredibly low density. Aerogel can have remarkable thermal insulation qualities while having a low density. High entropy refers to a class of materials containing multiple elements in roughly equal proportions. In the case of high entropy aerogels, these elements can be metals, non-metals, or a combination of both. The multiple elements create a complex atomic arrangement, creating unique structural and functional properties. The synthesis of a high-entropy aerogel intended for effective photocatalytic carbon dioxide reduction was the main goal of this research. Metal oxide precursors were carefully mixed in a high-entropy ratio using the sol-gel process to create a special composition that is intended to improve catalytic performance. A homogenous gel was produced containing a uniformly dispersed mixture of metal oxides with control over the sol gel process with extreme precision. After gelation, a freeze-drying process maintains the complex aerogel structure, avoiding breaking and guaranteeing peak performance. Copper oxide doped high entropy aerogel doped reduced graphene was formed by using hydrothermal method and tested for carbon dioxide reduction. The methanol yield from these two composites were compared. The characterization techniques such as SEM, UV-visible spectroscopy, FTIR, XPS, XRD, were applied to characterize the morphology and the structural properties of the high entropy aerogel. Once the synthesized aerogel was CD tested rigorously, its ability in reduction of CO_2 was tested under controlled conditions. Gas chromatography is utilized to analyze the resulting gas products, providing insights into the catalytic efficiency of the high-entropy aerogel and its composite CuO-HEAG@rGO. The yield obtained after GC results for the HEAG was 286.5 and for the composite CuO-HEAG@rGO was 1143.2

CHAPTER 1

INTRODUCTION

1.1 Porous materials

In addition to its composition, a porous material is usually defined by its textural characteristics related to pore structure. Several properties of the same material change when comparable in bulk, and yet in its porous form, Volumetric thickness, area of surface, accessibility, heat transmission, and rigidity fluctuate [1,2]. Only these changes can be justified if voids were added to the structure. For most of the solid materials, which we aren't normally aware of porous, most can be found to be some amount of porous (such as wood, earth, or concrete). Porosity is related to permeability in some practical cases, and the substances with interconnected pores along their volume instead of disconnected pores are more interesting for use in those applications that ensure fluid flow, adhesion, segregation, and catalytic processes, etc. Pure materials with pores with a lot of holes include feldspar, carbonized charcoal, ceramics, and so on. Furthermore, for other necessities, synthetic porous materials have been developed for many decades [3]. There are two broadly defined groups of pores characterizable by a view of whether the fluid can fill the substances.

1. Simple voids inside the bulk material that are closed pores and therefore not accessible to the fluid. These pores cannot be reached by the fluid, but they influence in several respects many of the properties of the material, including its density or mechanical strength.

2. The holes are then exposed to the outside of the substrate, and therefore the liquid can permeate into them. They are usually classified according to the number of openings (blind pores (having a single opening), by means of holes (with dual entrances), or linked pores (when a number of through holes inside the entire specimen are coupled together to form the bulk macrostructure). In general, open pore structures are more interesting from applications' point of view, as they increase the catalytic and the adsorptive capabilities of the material [4].

3. There are many classifications of open pores depending on the shape as cylindrical, conical, bottleneck, slit and irregular pores that can be used to classify open pores.

Under the laws of fluid mechanics, the liquids react variably based on the form of the pore [5].

In addition, pores can be labeled based on their size (Figure 1c). Pores are divided according small pores (pore dimension < 2nm), mesopores (2nm < pore diameter < 50nm), and large pores (pore dimension > 50nm) (IUPAC) [6]. The observed behavior of the liquids that enter or leave these tiny openings are classified differently based on their size intervals. The porous materials are finally classified on the basis of their chemical composition as natural, synthetic, or combined.

1. Significant chemical material with pores comprises organic frameworks with covalent bonds (The COF), several other types of large molecules (crosslinked or hyperbranched), large molecules with inherent permeability, and certain aerosols, such as starch aerogels.

2. The most prevalent inorganic porous materials include feldspar, ceramics, carbon as a component silica, and the majority of aerogels etc.

3. The components consist of two naturally occurring and chemical phases and are mixed material with pores. This group includes metallic organic structures (MOF) and operational inorganic porous materials such as "the graphene oxide aerosols."

1.2 Uses of permeable substances

The two most crucial properties of the permeable substance when considering applications that there is a void in its structure and that the surface area per volume is high. This is why they are often ideal candidates for applications for which these trademarks are useful.

1.2.1 Catalytic activity

In fact, when materials have high surface area, it is natural to think of catalysis as the first application. Because most of the chemical processes grow in a straight line with the catalyst's available dimension, both nanoparticles and porous media [7,8] are valid candidates to catalysis because the last presents a highly elevated and available reactive surface area. Heterogeneous catalysis is conventionally carried out on porous materials as reagents or reagent transporters. The majority of reagents are composed of pricey precious metals like silver, palladium, platinum, and precious metals, therefore, just a minimal amount of materials of catalyst should be used to hold as

much unblocking catalyst as possible [9]. Reactive tiny particles can be embedded into a porous matrix to maximize the reactive yield while using the least amount of material mass possible.

1.2.2 Isolation and retention

Porous materials have one of the most common applications in adsorption and separation. Nearly all the different applications are in fact adsorption and separations processes, from energy to chromatography. For example, charcoal was used in ancient times to cure gastrointestinal diseases as a treatment for this, and also disinfect the water in old Republic of India and Egyptian empire. Permeable substances are used for filtering out toxic gases and unfiltered water nowadays [11]. Porous materials are used for filtering out toxic gases [12] and unfiltered water [13] nowadays. However, while less breathtaking, those applications still remain as practical (but if any-thing even more so) as desiccants to overcome one of the most common processes in carbon-based chemistry and indeed in a large number of other unworthy ordinary natural phenomena for example damp clothes with silica gel bags [14]. Another one of the fields where porous materials are utilized is due to they have retention properties in the recognizing domain. The majority of chemical sensor types typically involve association by physical absorption or chemical absorption of the detected molecule. Using a substance with pores enables the active utilization of a significantly larger portion of the sensor's active surface in enrichment when all of these conditions are met [15].

1.2.3 Energy

Porous materials play a crucial role in almost all forms of energy related fields including capacitors as well as batteries, for example, such as electrodes, membranes, and solid electrolytes [16]. Day by day, these components have become essential for the electric automobile business. Materials with pores are involved as well in systems aiming at fuel storage where the use of such materials can decrease the chance of unpleasant outbursts while use and transit [17], such as for the creation of vehicles powered by hydrogen. Energy uses are also associated with heat exchange. In order to cool or heat a fluid [18], material with pores can transfer or supply energy to the liquid, gasoline, or liquid that travels through them. It can be used to recycle, disseminate, or concentrate heat energy in a variety of ways, making it useful in a variety of settings.

Examples of these include combustors, radiators, commercial boilers, and heat storage systems for energy [19].

1.2.4 Construction

For a number of reasons, porous materials are involved in the physical properties of building products. On the other hand, permeable substances can be used as an insulator of sound and heat [20]. Air is a good heat protector in general. Even if it doesn't radiate, it can still transport heat through circulation. The material's fragile, rigid exterior can either partially or completely divide the air pockets, but not enough to reduce the free routes of gas molecules [21]. Therefore, this series of wall gap walls significantly reduces the transfer of that heat. As with acoustic insulation [22], sound waves are absorbed by the porous material and then expelled in the same manner as with a chosen substance. Moreover, we can also find other types of energy absorption in material with pores, such as anti-vibrators and impact absorbance. The majority of porous materials are more flexible than bulk materials [23] and resemble sponges. As a result, they may take in and reduce the motion energy [24] from a hit, causing a significant reduction in the vibration that is transmitted to the air around them [25].

1.2.5 Drug

Permeable substances are used on a daily healthcare product such as medical implants, drug delivery systems, and clothing (bandages and dressings) [26]. Specifically, the drug delivery systems use these materials because they have pharmaceuticals in their pores and release them gradually by diffusion rather than dumping the entire dose into the medium at once, like regular pills do. The medicine's transporter is typically a biodegradable, and permeable polymer [27]. However, it may consist of a permeable biological chemical that, as the material breaks down gradually in the biological environment [28], releases regulated amounts of the medication. Alternatively, to create surgical implants like prostheses, porous materials are required. In order for the same existing tissue to infiltrate and anchor the pores, the implant needs them. As an example, In order to create a highly complicated surface area and get completely fixed to it, skeletal tissues can proliferate into the pores of bone prosthesis [29].

1.2.6 Bioreactors

Bioreactors are widely used in the generation of different chemicals and biological reactions with biological specimens, i.e., enzymes, bacteria, and microalgae. In food related application, bioreactors are used like yogurt, vinegar, natural pigments and alcoholic beverage production. Additionally, they manufacture medically related goods like the hormone insulin and enzymes. In other situations, the tiny algae and nutrients are actually required to be anchored to a porous surface to perform in a functional manner [30]. A porous medium (typically a ceramic) is therefore introduced into the bioreactor because, added to the bioreactor, it raises the enzyme or bacteria working area and therefore, it will be able to react with more enzyme or bacteria inside the bioreactor [31].

1.3 Aerogels

An essential kind of porous material that is thoroughly examined is aerogel. The "Aerogel is defined as a gel made of a tiny-pores solid with a gas as the dispersion phase" [32]. Unfortunately, the description is both too general and specific, as it does not include mesoporous aerogels, for example. The most often used definition in the literature at the moment is based on its characteristics: an aerogel is a solid, porous, low-density, dry framework of a gel that has been separated from its liquid component without losing volume [33-35]. The definition's main term is intact, specifically to completely distinguish aerogels from other goods linked to dry gel. This is especially important since different kinds of dry gels, such as cryogens or xerogels. This is especially important as an aerogel preserves the original solid structure of a gel while other varieties of deccicated gels, like cryogens or xerogels, don't. Most gels are made via sol-gel methods, in which a sol dispersed in a liquid accumulates to create a continuous three-dimensional network [32].

1.3.1 Hydrogel

When the liquid is either water or alcohol, separate techniques known as hydrogel or alcogel have been developed to remove (dry) the liquid from the gel [36], which can be done by space, thermal, or just exposure to environment, the liquid in the gel evaporates and produces a xerogel with a relatively high density. This method causes large capillary forces to occur during drying, which causes some pore walls to

collapse, greatly collasping the gel in the process significantly lowers the porosity and surface area of the material by altering its structure.

1.3.2 Cryogel

Freeze-Thaw, also known as lyophilization [37], involves sublimating the gel's liquid typically water under vacuum after it has been frozen. Since during the transpiration phase, there is zero liquid phase, this procedure eliminates the capillary tension created in the liquid-solid interface. A cryogel is the result. This process produces materials with very low densities because to low shrinkage levels. However, Cryogels are large pores materials that form structures due to their tight walls with less available domain because of their development process, which involves the solvent freezing inside the pores to create microcrystals. Because water expands when cold, shrinking the pore walls and resulting in big holes, this effect is particularly noticeable in cryogels made from hydrogels. In order to produce cryogels with varying results, various solvents such ethanol, acetonitrile, and dimethylsulfoxide have been studied [38]

1.3.3 Super critical drying

In order to prevent the capillary tension that causes the pores to collapse, supercritical drying [39] involves raising the gel's liquid to its perilous fact and then lowering the compression isothermally to create a gas. Aerogel is the end outcome. Hypercritical dewatering at the turning point of the solvent, typically a short-chain alcohol or acetone is how this liquid is removed in the majority of procedures. The threshold temperature is lowered by combining the liquid with CO_2, which has a low crucial temperature. The fluid can be substituted by Carbon dioxide, and CO_2 is the liquid to be removed. The shrinking of aerogels is often minimal yet detectable. Aerogels, which are formed from the same initial gel, are somehow denser than cryogels. In contrast to xerogels or cryogels, they essentially preserve the gel's original solid structure and mesoporosity since there is no hole development (or shrinkage) during the drying stage. This results in materials with surface area.

1.4 Discovery of aerogel

These days, aerogels constitute a significant field of study. The Web of Science (WOS) database contains around 19,000 papers published since the discovery of aerogel in 1931 to April 2022. Over the past ten years, the number of publications has really been growing dramatically. In 1931, S. S. Kistler reported the first minerals like alumina

and other substance aerogels made with hypercritical liquids [40] was reported by S. S. Kistler in 1931. Aside from Kistler's research, which continued to until the 1980s [41], academia along with business had mostly forgotten about aerogels. Many problems with the manufacturing procedures, which were time-consuming and costly, used dangerous substances, and had the potential to explode, can be blamed for this neglect. Furthermore, despite creating numerous aerogels with various arrangements, Kistler persisted in emphasizing the inclusion of silica aerogel, which would later go on to be the first to be sold commercially.

At the beginning of sol-gel chemistry in the 1970s, aerogel formation was given another go. In comparison to the original Kistler process, silica aerogels may be manufactured far more quickly, consistently, and with fewer flaws. Both industry and the scientific community were more interested in the issue of aerogel as a result of this accomplishment, which led to the continuous development of less hazardous and poisonous techniques. Supercritical CO_2 drying took the place of supercritical alcohol drying in the 1980s. The science of aerogels finally took off thanks to this last advancement and the creation of new varieties, such carbon aerogels made of pyrolyzed resorcinol-formaldehyde. These days, a variety of synthetic, natural, and hybrid materials are used to create novel aerogels every day [42].

1.5 The properties of aerogels

Many aerogels have been described recently, and each has a unique combination of properties. Assigning generic qualities to such a diverse collection of materials is difficult [43]. While most aerogels have low density, poor heat conduction, and wide dimension, A few of them are delicate or extremely light. Aerogels can be classified as felts, films, powders, or monoliths based on how they look. according to microstructures [44]: combined micro/mesoporous aerogel; mesoporous (2–50 nm); and microporous (< 2 nm). Chemical structure-based: composites, polymers, oxides, and hybrids. Aerogels' most notable feature is their incredibly low density, which is caused by their high porosity; their density is as low as 0.0011 gcm-3, and their porosity is above 99 percent [45]. Aerogels' low heat and sound conductivity, which makes them excellent insulators, is another of their very well-known characteristics.

1.6 Applications of aerogels

Given that aerogels can be customized and have a wide range of properties, In terms of uses, this material has undoubtedly evolved into a Swiss knife [46]. Despite the fact that aerogels have been around for forty years, they have only recently been used as new substitutes in commonplace products [47]. Certainly, advancements in technology and lower production costs would help new and intriguing applications to emerge.

1.6.1 Insulation

The most well-known use of aerogels is as a resistor; to explain this, P. Tsou stated in the 1980s, "You could take a two- or three-bedroom house, insulate it with aerogel, and you could heat the house with a candle, but eventually the house would become too hot." [48] Aerogel production was expensive back then, but in recent decades, methods have gotten cheaper, allowing for the development of commercial products. Today, aerogels can be used as heat resistors in Commonplace items like windows that boost home temperature regulation use materials similar to stone wool and quartz aerogel between their window panels [49]. The uses of aerogels in noise reduction should not be overlooked, despite the fact that thermal insulation is very different. Aerogel-containing commercial panels are 10–1000 times more effective in dampening [50] than other materials already in use. The rover traveling on the exterior of Mars [51] is insulated by aerogels, which help it maintain a steady working temperature in spite of the extremely high temperatures on the red planet. Aerogels are also employed on the wings of commercial airplanes to keep them from freezing during flights [52].

1.6.2 Storage

In the pharmaceutical industry, aerogels have been investigated as drug delivery systems. Controlled release [53] can be achieved by the aerogel's complex porosity structure or controlled breakdown. Aerogels' high porosity allows them to hold a lot of other materials in their pores. Applications involving energy storage have made use of carbon aerogels [54].

1.6.3 Environment

Already available to some of them for study: some aerogels can be considered as an instrument to preserve the environment [55]. One of the practical applications of a polymer derivative is in water remediation, especially oil recovery after spillage of oil. Aerogels can be made to be hydrophobic, so oil from a spill can be absorbed but the contaminating oil not seawater. The reutilizing of the bonded material also relies on the flexible behavior that can be added to the aerogel's properties [56].

1.6.4 Catalysis

Aerogels are perfect for catalytic applications because of their broad open dimensions and specially designed surface chemistry. This element can be included as a catalytic metal into the primary aerogel structure or deposited on the outermost layer of the pores [57]. When it comes to the first scenario, redox catalytic reactions [58] have been performed using zirconia aerogels [59]. In the second case, one can notice some studies where the aerogels are would be used as supports for the catalytic conversion of CO_2 and H_2 to methanol by adding copper/zinc oxide nanoparticles [60].

1.6.5 Energy

The energy sector can benefit greatly from the applications of aerogels. Batteries and supercapacitors, which require porous media in their construction, are currently the cornerstones of the future of energy storage. Aerogel between the anode and cathode is necessary in certain situations, whereas in others, either or both conductors contain porous material. Carbon aerogels are presently being developed for this purpose because they may be utilized as channels for the transport of ions in the battery (powerful capacitor) [61] or as an electric conductor adjacent to the collectors [62].

1.6.6 Hypervelocity particles capture

A curious application for which the aerogels' appearance seems to be soft, is high speed tiny materials capture, mainly galactic dust. For complex reasons, the problem of one of the most basic tasks in capturing cosmic dust, say, small particles traveling at high speed, is the ability to capture the dust that droplets into a solid when it hits the solid. Until now, to make it easier to recover this dust, space researchers as well as engineers have been searching for a substance that will capture these particles without causing any harm. The solution took the shape of silica aerogels. Usually, it takes a particle with a high velocity and conceals it in the substance without damaging it [63].

Additionally, the particle creates a small cone-shaped track when it slows down and stops. However, as silica aerogels are primarily transparent, this is easily forgiven [64].

1.6.7 Porous support

As previously mentioned, aerogel has a wide range of applications. However, aerogels' primary function in this dissertation work has been to support other materials [65]. The majority of the active ingredients in this thesis are made as micro or nanoparticulated powders. Generally speaking, any nanoparticle regardless of its composition is a little risky as it can enter the bloodstream straight through the skin and, in the instance of the lungs, the lung membranes. However, because the aerogel support is coupled to the volatilizing nanoparticles, it is not only possible to work alongside the usually dispersed components in a considerably better manner, but it is also possible to avoid dealing with them.

1.7 Supercritical CO_2

Supercritical fluids provide advantages over traditional organic solvents, which are more inappropriate, in contemporary laboratory and industrial applications. The most popular of these is SC CO_2, which is appealing because of its natural characteristics. Because it is inexpensive, non-flammable, and has relatively low critical requirements 304 K (31 ^{o}C) and 7,38 MPa (73.8 bar) for critical temperature and pressure it is regarded as a green solvent. Although it is typically restricted to low molecular mass and low polarization molecules, scCO_2 can act as a solvent [66]. The two phenomena listed below provide the solvent's characteristics: (i) CO_2 has a significant quadrupole moment despite being a nonpolar linear molecule [67] and (ii) a high quadrupole moment causes a Lewis acid property [68,69] The method can be made more versatile by adding co-solvents when a high degree of solvation is required. To increase the mixture's polarity, small volatile substances like ethanol, acetone, ethyl acetate, or other comparable substances are typically utilized as co-solvents in conjunction with CO2 [70].

1.8 High entropy aerogel

The major focus of research is the high entropy alloys (HEAs) that consist of at least 5 elements [71] on the basis of approximately 5–35 atomic % of five elements. These HEAs have excellent mechanical and chemical properties including high strength, high corrosion resistance, high hardness and good flexibility. Second, the exceptional

diversity of elemental composition, which is represented by almost any elemental combination to create a huge number of highly desired HEAs, has already been shown to be an extraordinary feature of HEAs. In addition, HEAs may also have the ability to confer excess structural stability [72] through their kinetic slow diffusion and thermodynamic entropy stabilizing effect. As promising electrochemical catalysts [73], high entropy alloy aerogels (HEAAs) have been developed with the beneficial combination of high entropy alloy and aerogel structure. However, due to the intrinsic thermodynamic instability and the variation of metal ion reduction potential, making 3D porous high entropy alloys with precise control is still a great challenge [72]. In this thesis, the synthesis of an aerogel for photocatalytic reduction of carbon is explained.

AIMS AND OBJECTIVES

Objectives

- To synthesize high-entropy aerogel
- To investigate the structural and optical properties of the product
- Characterization of high entropy aerogel by UV-visible, SEM, and XRD.
- To achieve maximum reduction of carbon dioxide by optimizing the High Entropy Aerogel.

CHAPTER 2

LITERATURE REVIEW

2.1 Introduction to High-Entropy Alloy Aerogels (HEAAs)

High entropy alloy aerogels (HEAAs), that are the combination of high entropy alloy and aerogels, have been attracting efforts to develop catalytic processes as platforms. Per their high activity and endurance, these materials have great promise for the CO2 reduction reaction (CO2RR) [74]. Some, such as PdCuAuAgBiIn HEAAs, achieve 98.1% maximum Faradaic efficiency for formic acid synthesis at -1.1 VRHE and nearly 100% Faradaic efficiency for C1 products. The extreme CO2RR performance of these HEAAs relies on strong interactions of many metals with the surface unsaturated sites that control electronic structures and enhances intermediate adsorption and desorption. Even though HEAAs have potential, conventional aerogels have been well researched for this purpose too.

2.2 Synthesis Methods for High Entropy Aerogels

2.2.1 Chelating Co-Reduction Strategy

The chelating co-reduction strategy is a recent and general method for preparing high-entropy alloy aerogels (HEAAs), performed at room temperature in a water phase. This technique introduces chelators to vary the reduction potential of metal constituents, successfully producing single-phase solid solution alloys such as AgRuPdAuPt HEAA [75].

2.2.2 Freeze-Thaw Method

The freeze-thaw method is utilized to prepare HEAAs as electrocatalysts for CO_2 reduction. This technique effectively creates single-phase HEAAs, overcoming issues related to differences in reduction potentials and metal miscibility [76].

2.2.3 In-Situ Carbothermal Reduction/Partial Sintering Technique

A novel method of synthesis of (Ti0.167Cr0.167V0.167Mo0.167Nb0.167Ta0.167) aerogels in-situ carbothermal reduction/partial sintering was used at 1773 K. The development of multi component complex aerogels is shown to be promising by this technique [77].

2.2.4 Supercritical Carbon Dioxide Synthesis

Supercritical carbon dioxide ($scCO_2$) is an effective and environmentally friendly solvent for synthesizing aerogels. It has been successfully used to produce GO aerogels from GO dispersions made up of ethanol at moderate conditions (333 K and 20 MPa) [78].

2.2.5 In-Situ Reduction and Freeze-Drying Process

The in-situ reduction followed by the freeze-drying process has been used to synthesize alloy aerogels. This method enables the development of aerogels with desired Sn content and three-dimensional structures of uniformly dispersed nanocrystals and interconnected channels [79].

2.3 Hybrid Aerogels and CO_2 Capture

Combining various materials, hybrid aerogels have demonstrated superior CO_2 selectivity and adsorption capabilities, making them a promising tool for climate change mitigation. This demonstrates how aerogel-based materials can be used in a variety of ways to address CO_2-related issues, including capture and reduction strategies [80]. Because of its special qualities and flexible active sites, the synthesis of (HEAs) for electrocatalytic applications has attracted a lot of interest. In several electrocatalytic processes, such as the CO_2RR, HEAs have demonstrated exceptional performance [81]. Because HEAs have several neighboring elements, this opens up the possibility of creating unique and flexible active sites that may be tailored for particular uses by carefully choosing element composition and arrangement.

2.4 Characterization and Properties

2.4.1 Microstructure and Morphology

High-entropy aerogels generally exhibit a non-grain structure with nanometer/micrometer grain phase pores. For example, the 6-HETMC aerogel shows grain phases of 100–300 nm and pore ranges of 0.2–10 μm [82].

2.4.2 Surface Area and Porosity Analysis

The Brunauer–Emmett–Teller (BET) method determines the specific surface area of aerogels, with some of them possessing surface areas as high as 282 m^2/g.

2.4.3 Thermal and Mechanical Properties

Characterization of thermal conductivity and compressive strength has revealed that HETMC aerogels possess low heat conductivity and excellent mechanical characteristics.

2.4.4 Performance of High Entropy Aerogels

High entropy aerogels (HEAs) are emerging as promising materials for CO_2 reduction due to their unique structural properties and catalytic capabilities. They combine the benefits of aerogels and high entropy alloys, including high surface areas, tunable pore sizes, and enhanced catalytic activity. This development addresses the urgent need for sustainable solutions for carbon capture and utilization.

2.5 Characterization Methods for High Entropy Aerogels

2.5.1 Methods of Microscopy

The structural characteristics of the aerogels such as pore size distribution, nanocrystal morphology and three dimensional porous structure is studied by HRTEM and FESEM.

2.5.2 X-ray Diffraction Analysis

Crystalline structures and phases of high entropy aerogels are also analyzed by X ray diffraction with measurement of their structural integrity and composition [83].

2.6 High Entropy Materials (HEMs) and Environmental Applications

Remediating wastewater and converting and storing energy are just two of the environmental issues that high entropy materials (HEMs), including HEAs, have shown promise for solving. HEMs have proven to be catalytic in the context of CO_2 reduction, using both photocatalytic and electrocatalytic pathways to transform CO_2 into value-added compounds [84]. This adaptability highlights how high-entropy materials can be used to address a variety of environmental sustainability issues. Since their discovery, aerogels, which are distinguished by their exceptional qualities because of their high porosity, have been the focus of much research. Especially carbon aerogels, with their huge specific inner surface areas and strong electrical conductivity, have shown promise as fuel cell and supercapacitor electrodes. These characteristics make carbon aerogels potentially useful for applications involving the reduction of CO_2; however, more study is required to fully explore this potential [85].

2.7 High-Entropy Alloys (HEAs) and Their Properties

Because of their unique and useful properties, high-entropy alloys were created. which include good low-temperature plasticity, exceptional thermal stability, and the capacity to overcome the strength-ductility trade-off [86]. These characteristics, along with the capacity to create chemical disturbance, render HEAs appealing for a range of uses, such as catalysis. The examination of HEA synthesis, production, and processing techniques offers important information for creating HEAAs that reduce CO_2. Because of the customized composition and disordered arrangement of HEAs and high-entropy compounds, electrocatalysis on these materials has become a promising subject.

2.7.1 Computational Techniques and HEA Catalyst

Nevertheless, the intricacy of multicomponent systems poses difficulties in comprehending the specifics pertaining to active sites and intrinsic activity. Density functional theory (DFT) and other computational techniques have been used to find and create the best HEA- and HEC-based catalysts for a variety of electrocatalytic energy conversion processes, including the CO_2RR. Combining the benefits of aerogels and high-entropy alloys, HEAs have become attractive platforms for catalytic processes. These materials are especially well-suited for carbon dioxide reduction reactions (CO_2RR) because of their special qualities, which include variable pore size, customizable framework, vast surface area and a plethora of active locations. The miscibility behavior and varying reduction potentials of various metals are obstacles to the creation of HEAAs. However, recent studies have shown that HEAAs can be successfully fabricated utilizing techniques such as the freeze-thaw method [87].

2.7.2 Specific Examples and Performance of HEAAs

PdCuAuAgBiIn HEAAs, for example, have demonstrated excellent CO_2RR performance, with near-total FE of 100% for C1 products and a maximum FE of 98.1% for formic acid production at -1.1VRHE. The strong metal-surface unsaturated site interactions control the electronic structures and optimize intermediate adsorption and desorption, resulting in a synergistic effect that improves the production of valuable products such as formic acid [88]. These advancements have improved our knowledge of HEA-related reaction processes, constituent element interactions, and active sites.

Because of their capacity to catalyze a wide range of redox processes, high-entropy materials (HEMs) including HEAs, have demonstrated potential in solving environmental concerns. Their possible uses include energy conversion and storage as well as wastewater cleanup. HEMs have proven useful in reducing carbon dioxide through photocatalytic and electrocatalytic pathways to produce value-added products. High capacitance, electrical conductivity, and thermal stability are among the special qualities that set HEMs apart and make them useful parts for achieving essential energy needs. However, a greater comprehension of the underlying principles driving their catalytic and electrochemical behaviors is necessary to optimize HEM performance in catalysis and energy storage.

2.8 Research Focus and Developments in Aerogel Science

Aerogels have been thoroughly researched for a variety of applications, including CO_2 capture and reduction. They are well-known for their exceptional qualities owing to their high porosity. Carbon aerogels, in particular, have showed potential as fuel cell and supercapacitor electrodes due to their large specific inner surface area and strong electrical conductivity [89]. Recent advances in aerogel science have concentrated on structural characterization and property measuring methods, as well as rapid supercritical and ambient pressure drying processes. These developments have aided in the creation of more effective and customized aerogel materials for certain uses, such as the reduction of CO_2.

2.9 A Novel Material for Thermal Barrier Coatings with Enhanced Thermal Insulation and Stability

Because of their potential applications in thermal barrier coatings (TBCs) for gas turbines, such as high-entropy oxides (HEOs) and high-entropy ceramics (HECs) have been attracting more and more attentions. Studies like this indicate that for high temperatures there is a need for new TBC material with better thermal stability and lower thermal conductivity than is the case with conventional materials, like yttria stabilized zirconia (YSZ), the latter of which possesses limitations. A new high entropy ceramic (La 0.2Nd 0.2Sm 0.2Eu 0.2Gd 0.2) $2Ce_2O_7$ is proposed by the authors that exhibits promising thermal insulation properties and phase stability at elevated temperatures. SEM and TEM were used to analyse the microstructure and elemental distribution of synthesized (La 0.2 Nd 0.2 Sm 0.2 Eu 0.2 Gd 0.2) 2 Ce_2O_7, which

show homogeneous element distribution and defective fluorite structure. Thermal properties including the thermal conductivity and thermal expansion coefficient (TEC) were measured: low thermal conductivity of 0.92 W•m −1 •K −1 at 1400 °C and high TEC of 12.0 × 10 −6 K −1. This study places emphasis on the cocktail effect of the multicomponent elements in phonon scattering and thus on the occurrence of good thermal insulation of the material, due to the role of the oxygen vacancies. The research has shown that (La 0.2 Nd 0.2 Sm 0.2 Eu 0.2 Gd 0.2) $2Ce_2O_7$ exhibits exceptional thermal insulation properties with a very low thermal conductivity [90] associated with the enhanced phonon scattering. The factors of reducing thermal conductivity are the high concentration of oxygen vacancies, and the randomness distribution of rare earth ions. The results presented in this work are critical to develop high entropy ceramics as viable TBC materials overcoming the challenges associated with traditional materials.

2.10 High Entropy Oxides (HEOs) as Advanced Electrocatalysts for Water Oxidation Reactions

Main advantage of water oxidation reaction (WOR) hydrogen production method is that it is a cleaner approach than fossil fuel production with higher energy conversion efficiency. Recent advancements in electrocatalysts, particularly high entropy oxides (HEOs), show promise in enhancing the kinetics of electrochemical oxidation reactions, crucial for efficient water splitting. The study focuses on synthesizing and characterizing equiatomic and non-equiatomic HEOs for their potential as effective electrocatalysts in WOR. Synthesis of HEOs HEOs were synthesized using a sol-gel method, where metal precursor solutions were mixed and heated to form a viscous gel, followed by drying and calcination. The synthesis process varied for equiatomic and non-equiatomic compositions, with specific ratios of metal precursors to achieve desired properties. The resulting powders were characterized to confirm the formation of high entropy materials suitable for catalytic applications. Instrumentation Characterization of HEOs was performed using FTIR and XRD techniques to analyze structural and compositional properties. Electrochemical measurements were conducted using a three-electrode system, with a glassy carbon electrode modified with HEOs for cyclic voltammetry. The setup allowed for the assessment of electrocatalytic performance in water oxidation reactions. Electrochemical Studies Cyclic voltammetry (CV) was employed to evaluate the electrocatalytic properties of

HEOs, revealing their redox behavior and efficiency in WOR. The presence of methanol significantly enhanced charge transfer and reduced onset potential, indicating its role as a facilitating agent in the electrochemical process. Non-equiatomic HEOs demonstrated superior catalytic performance compared to equiatomic counterparts, particularly with higher aluminum content. Kinetics of Water Oxidation over HEOs The study estimated diffusion coefficients and rate constants for the water oxidation process using Randles-Sevcik and Reinmuth equations. Results indicated that smaller particle sizes in HEOs correlated with better electrocatalytic performance, with non-equiatomic compositions showing higher current densities. The performance of HEOs was compared favorably against state-of-the-art catalysts, suggesting their potential for further electrochemical applications. The synthesized HEOs exhibited stable catalytic performance over a period of 1-2 days, maintaining efficiency in water oxidation reactions. This stability indicates the practical applicability of HEOs in long-term electrochemical processes, enhancing their viability as electrocatalysts. make a single heading for this data [91].

2.11 Enhanced CO_2 Capture Using K_2CO_3-Impregnated Carbon Aerogel Nanocomposites Under Moist Conditions

The paper addresses the critical issue of rising atmospheric CO_2 levels due to fossil fuel combustion, which contributes to climate change and environmental degradation. Alkali metal carbonates, particularly K_2CO_3, are proposed as effective and low-cost sorbents for CO_2 capture, especially when supported on nanoporous materials like carbon aerogels. The results aim at increasing CRB capture efficiency and lowering regeneration temperatures when K_2CO_3 is incorporated in the mesopores of carbon aerogels. An investigation on the synthesis of carbon aerogels (CAs) from resorcinol using different molar ratios of resorcinol to water, followed by polymerization and supercritical drying to generate nanoporous structures was conducted. K_2CO_3 was impregnated into the nanopores of the CAs using an aqueous solution, and the resulting nanocomposites were characterized for their structural properties and CO_2 capture capabilities. The preparation involved careful control of temperature and pressure during carbonization and drying processes to maintain the integrity of the nanoporous structure. The structural properties of the CAs and K_2CO_3 nanocomposites were analyzed using N_2 adsorption measurements and thermogravimetric analysis (TG-DTA) to determine pore sizes and CO_2 capture capacity. To verify the formation

of $KHCO_3$ and the regeneration process of the CO_2 nanocomposites, XRD is used. X-ray diffraction (XRD) was employed to confirm the formation of $KHCO_3$ during CO_2 capture and to assess the regeneration process of the nanocomposites. The amount of CO_2 captured was quantified using a CaO solution-precipitation method, ensuring accurate measurement of the sorbent's performance. The study found that the K_2CO_3 nanocrystals exhibited high reactivity and lower regeneration temperatures compared to bulk K_2CO_3, enhancing the efficiency of CO_2 capture. The water adsorption behavior of the nanocomposites was complex, influenced by both the hygroscopic nature of K_2CO_3 and the physical adsorption properties of the CAs. The CO_2 capture capacity of the nanocomposites was significantly higher than theoretical values, indicating their potential for effective CO_2 sorption under moist conditions. CO_2 Capture Ability under Moist Conditions The xCA-KC nanocomposites demonstrated a CO_2 sorption capacity of 2.68 mmol/g-sorbent, surpassing the theoretical capture capacity of K_2CO_3. The capture process was rapid, reaching equilibrium within minutes, and was influenced by the impregnation rate of K_2CO_3 into the mesopores. The results suggest that the nanocomposites can effectively capture CO_2 in humid environments, which is critical for practical applications make single statement for this data [92].

2.12 Enhanced CO_2 Adsorption Using Nitrogen-Doped Carbon Aerogels Synthesized with Urea

Global warming is primarily driven by greenhouse gas emissions, particularly methane and carbon dioxide, which pose significant environmental and socio-economic risks. The study explores the potential Using nitrogen-doped porous carbon compounds for CO_2 capture highlighting their high adsorption capacity and stability compared to traditional adsorbents. The research introduces a novel method for synthesizing N-doped carbon aerogels using urea and resorcinol-formaldehyde, aiming to enhance CO_2 adsorption through improved surface nitrogen functionalities. The synthesis involved a sol-gel polymerization process, where formaldehyde was added to a mixture of resorcinol and urea, followed by drying and pyrolysis under nitrogen atmosphere. Different samples were created by varying the molar ratio of resorcinol to urea, denoted as AU0, AU1, and AU2, to investigate the effects on structural properties. Acetone was chosen as the drying solvent to minimize shrinkage during the drying process of the resorcinol-formaldehyde-urea gels. The characterization of

the N-doped carbon aerogels included measuring total pore volume and CO_2 adsorption isotherms, revealing significant differences in nitrogen content and surface area among the samples. The study noted that increasing the urea content led to a decrease in both micropore volume and overall porosity, impacting the adsorption capacity. Limitations in characterization approaches were noted, such as the absence of scanning electron microscopy pictures, which may have offered deeper insights into the material's structure CO_2 adsorption. The N-doped carbon aerogels demonstrated superior CO_2 adsorption capacities compared to non-doped counterparts, with AU1 showing the best performance despite lower nitrogen content. The study confirmed that the presence of basic nitrogen groups enhances CO_2 adsorption through strong interactions between CO_2 molecules and the nitrogen functionalities. The findings suggest that optimizing the nitrogen content and pore structure is crucial for improving the efficiency of CO_2 capture in these materials. The research concludes that increasing the amount of urea in the synthesis of N-doped carbon aerogels significantly enhances CO_2 adsorption compared to non-doped variants. The study emphasizes the importance of nitrogen doping and pore structure in developing effective adsorbents for CO_2 capture applications make a single heading for this data [93].

2.13 High Entropy Alloys for Enhanced Oxygen Evolution Reaction (OER) Activity and Stability in Water Electrolysis

Particularly, the study centers on the development of cost effective and efficient electrocatalysts for room temperature water electrolysis (WTE), especially the oxygen evolution reaction (OER) which is needed for production of hydrogen. To effectively promote activity and durability of carbon fiber (CF) based high entropy oxide (HEO) catalysts, tools including a novel in situ synthesis method (carbothermal shock, CTS) are introduced. The process is achieved by drop casting metal chloride salts on carbon fiber paper and then rapidly heating them with Joules to form HEO nanoparticles directly on the substrate without the need of separate media to stabilize them. XRD and SEM confirm the formation of HEO nanoparticles with a uniform way, and solidly contact on the carbon support. Electrocatalytic performance was also examined for a series of different HEO compositions and it was found that addition of elements such as Cr, Mn, and V improves OER activity, while the best performing catalyst reaches an overpotential of 220 mV. A significant role of oxidation states of transition metals

in the catalysts for OER is emphasized through the study, where Cr was found to have an unprecedented impact. The HEO catalysts were shown to perform with stable performance in durability tests and in some cases to demonstrate improved activity, while other known catalyst types suffering from degradation can. The exceptional stability of the FeNiCoCrV catalyst was demonstrated and two orders of magnitude better than the commercial IrO_2 catalyst showed its potential for commercial applications. Enhancement in OER Activity and Origin of Stability Technologies to enhance OER activity are revealed by the formation of higher oxidation states in the active metals to promote better metal oxide hybridization and decrease the energy penalty for the reaction. The study suggests that during operation, derivatives of the single-atom to nanoparticle phase diagram results in single atom catalysts and even smaller nanoparticles, which enhances catalytic performance. Cr incorporation into the HEO catalysts enhanced the OER activity and stability in a way that was fundamentally enhanced by metal, carbide bond dynamics that arise from the synthesis of the HEO materials. Future research is suggested to explore other alloying ratios and investigate different ratios to optimize catalyst performance and longevity as the dissolution of less stable elements is now likely to have an indirect effect on overall activity [94].

2.14 Future Directions in HEAAs and Aerogels

Among these potential solutions to the development of effective CO_2 reduction catalysts are HEAAs or high-entropy alloys and aerogels. The recent development of high-entropy alloy aerogels (HEAAs) as platforms for catalysis has their advantages in the properties of high-entropy alloys and aerogels. The use of high entropy alloy aerogels (HEAAs) enables creation of materials with increased catalytic activity, selectivity and stability. These materials have a high activity and endurance, and they have considerable potential to be used as catalysts for the carbon dioxide reduction reaction (CO_2RR). For example, PdCuAuAgBiIn HEAAs exhibited superb performance in CO_2RR with faradaic efficiency of up to 98.1% on formic acid synthesis at -1.1VRHE, and approaching 100% for C1 products. These remarkable performances are due to strong interactions between various metals on one hand, and surface unsaturated sites which dictate electronic structures and maximize the adsorption and desorption, on the other hand. Interestingly, there already is a lot of research done with general aerogels for CO_2 collection, so HEAAs have potential for

CO_2RR. Due to their variable pore size, adaptable structure, large surface area and much active sites they are effective CO_2 adsorbents. Therefore, aerogels' ability to both capture and reduce CO_2 is critical for adapting to climate change issues. High-entropy alloys (HEAs) are a material consisting of 5 and above (almost) equal amount of elements. They have been the object of considerable attention due to their extraordinary strength, good ductility and corrosion resistance. With these substances, we have shown a remarkable feature in electric catalytic processes, such as CO_2RR. Being able to have the capability to have a number of adjacent components and produce unique and flexible active sites that can be tuned for specific purposes through better element composition and arrangement, promising HEAs. Among them have been remedies for environmental problems such as by remediating wastewater and convert and store energy, all served by what are known as high entropy materials (HEMs) such as HEAs. The various redox processes that they are able to catalyze with their electrocatalytic and photocatalytic routes are their CO_2 reduction to compounds of value. HEMs and therefore, HEAAs are good candidates for multipurpose environmental applications, due to their adaptability. A great deal of research has been carried out on aerogels, the extremely high porosity of which has made them exceptional, since the late 1980s. Because of their large specific inner surface areas and good electrical conductivity, carbon aerogels have received particular interest as electrodes for fuel cells and supercapacitors. The properties described here may have utility for the development of HEAAs for CO_2RR applications. This has inspired the development of HEAs because the possibility exists to engineer the chemical disorder present in HEXs to highlight new structural and physical properties. In the last 20 years, considerable work has been carried out to understand of the special features of HEAs, including their good thermal stability as well as their ability to circumvent upper toughness limit.

CHAPTER 3

METHODOLOGY

3.1 Materials

All reagents were used as purchased with no further purification. Metal salts precursors i.e, Cobalt chloride, Zinc nitrate dihydrate, Ammonium molybdate tetrahydrate, Sodium tungstate dihydrate, Sodium selenite, Iron chloride hexahydrate copper nitrate trihydrate, were purchased from Sigma Aldrich. Distilled water, deionized water, and ethanol were used as solvents. Polyvinyl alcohol as a binding agent, TEOS (tetraethyl orthosilicate), and sodium hydroxide were used in the reaction procedure. GO was synthesized by the Hummer method.

3.2 Apparatus

Magnetic stirrers, reaction vessels with appropriate sealing mechanisms, a centrifuge for separating particles, molds, and supercritical drying apparatus. UV lamps or other light sources, gas chromatography (GC) for gas analysis, characterization tools (SEM, UV-visible spectroscopy, PL, FTIR, XPS, and XRD.

3.3 Synthesis of high entropy aerogel

High entropy aerogel was synthesized via the sol-gel method based on the reported procedure in the literature with some modifications [95]. Briefly, 0.8 mmol of each metallic salt was added to 50 mL of the beaker from which the cobalt chloride, sodium selenite, and zinc nitrate dihydrate were dissolved in 4.5 mL of deionized water separately. Ammonium molybdate tetrahydrate, sodium tungstate dihydrate, and polyvinyl alcohol were dissolved in 4.5 ml of ethanol. All the suspensions were then mixed drop-wise together and stirred for about 15 minutes to make a homogenous mixture. We verified the homogeneity of the solution by heating it up 50 C for 10 min, turn off the heat, and add 4.5ml TEOS to the solution. Stirring was continued until the solution turned into a sol. The pH of the solution was maintained at 7 by adding Sodium hydroxide. Then the sol was transferred into the molds and placed into the water bath at 0 degrees for 3 hours. For gelation, the sol was then left for 6 days to convert into a gel. After 6 days, the gel was soaked in ethanol several times to preserve its structure, and the gel was passed through freeze drying to remove all the solvent

from the gel and make it an aerogel, the lightest of all gels. Aerogel was then calcined at 750 °C for 3 hours, and the crystalline powder of high entropy aerogel was obtained. Sample was then subjected to photocatalytic reduction Before and after calcination, aerogels are shown in Figures 10,11.

3.3.1 Synthesis of CuO-HEAG@rGO Composite

After that, the hydrothermal synthesis method was applied for the synthesis of the composite. The aerogel was taken in a beaker containing 50 ml deionized water and stirred until completely dissolved. 1g GO, 0.2M copper nitrate trihydrate, and 1g high entropy aerogel was added into the 3 different beakers. Each beaker contained 50 ml of deionized water and was dissolved through the ultrasonication method for 30 minutes. After the preparation of all the solutions, these solutions were transferred to the hydrothermal and set temperature of 140°C for 4 hours. After that sample was washed with ethanol and deionized water several times and dried in a drying oven for 24 hours at 80 °C. After drying sample was calcined at 500 °C for 3 hours, sample was turned into black powder and used for photocatalysis.

Figure 3.3: (a) Before calcination (b) After calcination

3.4 Photocatalysis for carbon dioxide reduction

The use of UV light to drive a chemical reaction that photocatalytically converts CO_2 into a useful product such as methanol is known as photocatalysis of carbon dioxide (CO_2). As a photocatalyst, the prepared aerogel was used for this process since it absorbs photons from the light source and generates excited electrons and holes. The reduction of CO_2 involves participation of these excited electrons while holes drive the oxidation of water to produce protons and oxygen. On the catalyst surfaces, the protons and excited electrons combine with CO, which leads to the production of fuels.

The figure shows that 0.5g photocatalyst has been added in to 100 ml deionized water after all the setup completed, and put in to the flask. To do this, only the carbon dioxide was then passed and the solution was then magnetically stirred for 30 minutes. The zero sample was then collected by using a syringe transferred into the sample voil and then the UV lamp was opened after an hour 1st sample was collected temperature was 60 degrees the reaction continued for 2nd hour and then again 2nd sample was collected the reaction was continued for straight 6 hours and the sample was collected after every passing hour. After 6 hours, the reaction was then stopped, and the samples collected were then subjected to Gas Chromatography to measure the conversion of carbon dioxide into a useful product i.e. methanol.

Figure 3.4: Lab-build Photocatalytic reaction chamber

CHAPTER 4

RESULTS

UV-visible spectroscopy (Agilent Technologies Cary 60), photoluminescence spectroscopy (Agilent Cary Eclipse Florescence spectroscopy), and Fourier transform infrared spectroscopy were used to examine optical properties.

4.1 Ultraviolet-Visible Spectroscopic Analysis

The UV-Vis spectroscopic analysis for HEA gel was performed in order to determine its optical properties, its interaction with copper oxide (CuO), as well as with reduced graphene oxide (rGO). The HEA gel revealed a typical absorption peak of around 394.5 nm. This was attributed to the π-π* electronic transitions inside of the molecular structure [96].

A clear shift within the absorption peak was observed after incorporating copper oxide (CuO) in conjunction with reduced graphene oxide (rGO). The composite material displayed an original novel absorption peak at 532.3 nm. This redshift suggests a powerful connection involving the HEA gel and the CuO/rGO parts, caused by the creation of charge transfer complexes or better electronic joining inside the combined form. The shift equally signifies substantially improved light-harvesting properties. These properties can be additionally helpful for quite broader applications, such as photocatalysis catalysis [97].

So the band gap of HEA gel, first calculated according to the Tauc equation and also consistent with the fact that HEA gel is a semiconductor. Although this reduces to 1.5 eV band gap, once copper oxide and reduced graphene oxide were incorporated into the composite. The large decrease in band gap is important because it means readily facilitating electron transitions through the composite, which is important for its enhanced photocatalytic activity.

Furthermore, the addition of the reduced graphene oxide enhances the charge separation within the composite. Electrons on graphene have high electrical conductivity to enable electron transfer, thereby lowering the recombination rates of

the generated pairs of electron and hole during the photocatalytic reactions. The synergy between the system consisting of HEA gel, CuO, and rGO further improves the photocatalytic performance of the material as a whole.

(a)

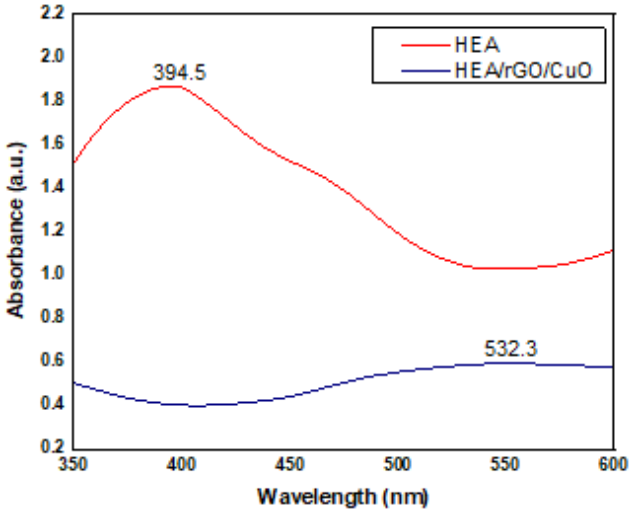

(b)

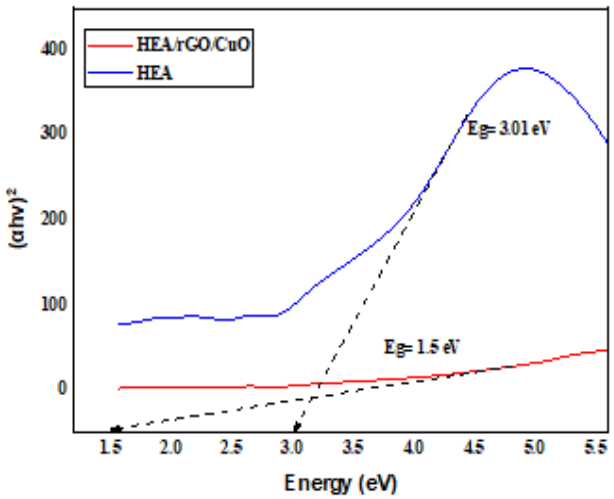

Figure 4.1 (a). The visible portion of the UV-Vis absorption spectrum. (Fig) exhibits a broad absorption band, suggesting a bandgap of roughly 1.5 eV compared to the HEAG 3.05 eV (b).

4.2 Fourier transform infrared spectroscopy analysis

Under infrared radiation, all molecules and chemical structures reveal individual spectral fingerprints which are uniquely identifiable. FTIR spectroscopy confirmed the identification of functional groups found in produced samples which the scientist presented through Figure 6. The FTIR spectra helped to reduce oxygen based groups in GO into rGO as illustrated in Figure. Interacting infrared band at 3400 cm^{-1} represents hydroxyl (O-H) groups which are located in unoxidized regions of graphitic frameworks [98]. The FTIR analysis shows that some tiny peaks located at 3451 cm^{-1} point to O-H stretching vibrations but attributed to either surface hydroxyl groups or adsorbed water [99]. The surface of this material reveals hydroxyl group O-H stretching vibrations at 3450 cm^{-1} through the peak formation. Research shows that aliphatic hydrocarbon C-H stretching vibrations produce a peak at 816.79 cm^{-1} [100]. The H-O-H bending vibration detected at 1637 cm^{-1} represents water located on the surface of the material [101]. The vibrational signal at 1475.01 cm^{-1} represents carbonate species as well as symmetric C-O bond stretching vibrations [102]. Research indicates that the two distinctive absorption bands at 682.05 cm^{-1} and 749.4 cm^{-1} [103] show absorption characteristics of the Cu-O-Cu and Cu-O-Se stretching modes where strong coupling occurs [103]. HEAG, CuO and graphene in ternary hybrid materials.

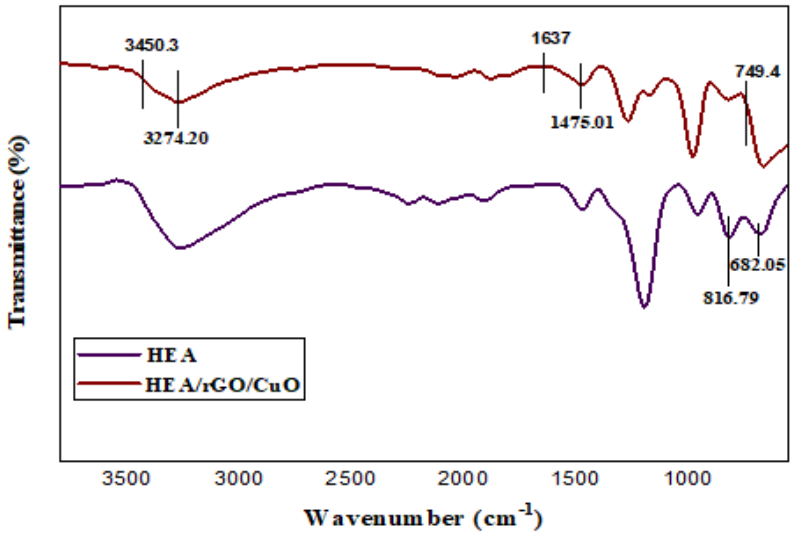

Figure 4.2: Several important vibrational modes revealed by the FTIR spectrum

4.3 Photoluminescence Analysis

To examine the optical behavior of the high-entropy aerogel and the impact of adding CuO and rGO on its emission characteristics, the photoluminescence (PL) properties of the material were examined. The lower PL intensity was correlated with lower recombination rate and prolonged timespan for photogenerated charge carriers. By adding copper oxide (CuO) and reduced graphene oxide (rGO), the observed photoluminescence (PL) peak shift in high-entropy aerogel (HEA) shifts from 535.34 nm to 571 nm, reflecting changes in electronic structure, defect states, and interfacial interactions [104].

The pure high-entropy aerogel's PL emission at 535.34 nm (green region) most likely results from:

1. Defect-mediated recombination: Because of their multi-component atomic structures, high-entropy materials frequently display many defect states (such as oxygen vacancies and lattice distortions). For photoexcited carriers, these flaws serve as radiative recombination sites.

2. Band-edge transitions: As observed in similar systems, such as polyurethane aerogels with nanoscale grains, the HEA's inherent bandgap may coincide with transitions emitting at approximately 535.34 nm.

The redshift (to the yellow-red area at 571 nm) implies structural alterations and electronic interactions in the composite. Among the important mechanisms are:

3. Defect-State Design

Introduction to CuO: The creation of mid-gap defect states by Cu^{2+} ions, such as oxygen vacancies and Cu^{+}/Cu^{2+} redox pairs, lowers the effective bandgap and permits emission at longer wavelengths.

Contribution of rGO: The Sp^2 conjugated domains and defect sites (such as vacancies and edges) introduced by reduced graphene oxide hybridize with the electronic states of HEA, further red shifting PL.

4. Charge Transfer at Interfaces

CuO/rGO and the HEA create heterojunctions that facilitate interfacial electron transport. This stabilizes lower-energy excited states and slows recombination, as seen in Cu_2O/rGO composites [105]. By lowering the exciton binding energy through the hybrid system's extended conjugation (by rGO's π-network), red-shifted emission is preferred.

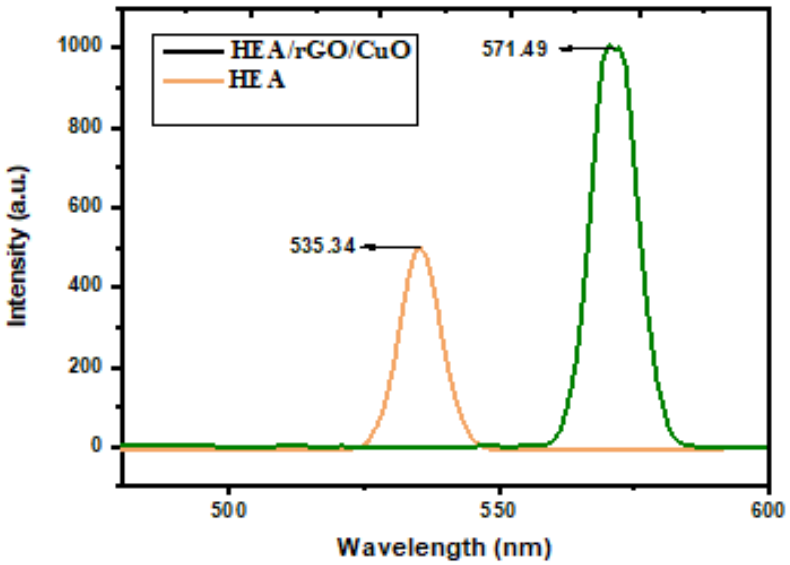

Figure 4.3: PL emission spectra of HEAG and HEAG@CuO@rGO composite.

Structural characteristics were investigated using scanning electron microscopy (SEM) and X-ray photon spectroscopy.

4.4 Scanning Electron Microscopy

The morphology seen in SEM pictures most likely consists of a mix of uniformly distributed or aggregated copper-based nanoparticles and smooth rGO sheets. The composite's size of 165.60 nm indicates that it contains a considerable amount of nanoscale characteristics, which can improve its efficacy and reactivity in processes like photocatalysis. Enhancing photocatalytic activity requires charge transfer, which is facilitated by the interaction between CuO and rGO. Because of its semiconductor qualities, HEA gel may potentially aid in this interaction by offering more active areas for reactions.

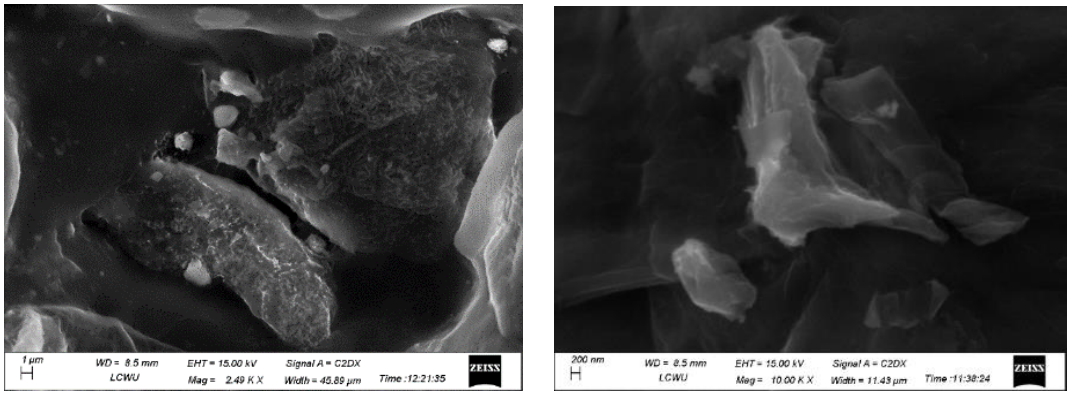

(a) (b)

Figure 4.4: (a) SEM image of HEA gel nanocomposites, (b) SEM image of HEAG@CuO@rGO nanocomposites.

4.5 X-ray Photon Spectroscopy analysis

The chemical composition of CuO-HEAG@rGO nanocomposites was then determined by XPS. A CuO-HEAG@rGO nanocomposite was produced and the XPS survey spectrum of Fig 6 showed peaks from Cu, Se, O, and C. Fig 6(b) is a moment in time and presents the multiple peaks associated with a peak such as 932.22, 940.13, 942.04 and 952.37 eV. It is likely that the peak at 932.22eV is related to Cu (I) oxide (Cu2O). This indicates 940.13 eV as the Cu (II) oxide (CuO) peak. The transition in the oxidation state of copper oxide is centered at 942.22 eV, and this is the peak. XPS spectra of Cu2p3/2 clearly indicate Cu+ oxidation to Cu+ and Cu+2 at the same time. The selenium 3d core level binding energy of 54.37 Ev confirms a lattice Se-2 fig 5(c) while the peak at 60.74 eV has oxidation state of selenium. Fig 5(d) shows that the C1s spectrum of CuO-HEAG@rGO nanocomposite indicates C1s spectra of carbon in the composite at 285.6 [106]. The O1s scan showed two major peaks at 530.7 and 533.2 eV corresponding to C–O and O–H (Fig.5(f)) respectively [107], meanwhile XPS spectra of molybdenum typically assess the Mo 3d region because the peaks separate well because of spin-orbit splitting while the typical molybdenum oxidation states exhibit Mo $3d_{5/2}$ binding energies at 229.3 eV (screened) and 231.0 eV [108]. Study results demonstrate a good correlation by monitoring the peak positions of Co2p at 781 and 796 eV. The BEs of 7779.6 eV have been confirmed for Co(III) in perovskite materials and Co(Il) in CoO sample displays 780.3 eV. Lab-scale investigation indicates that the surface reduction process has decreased the Co content

on 3LSC by detecting changes in the Co 2p peak position. The low dissociation energy of CoO leads to a natural consequence of becoming reduced due to the high reduction ability during calcination. [109]. shows the W 4f and O 2p spectra, the survey spectrum, and the valence band spectrum of the nano-tiles. A graphic representation of W 4f core levels appears in Figure 6a. The measured spectrum contains two main doublets alongside another peak which represents the photoelectrons emitted from W 5p orbitals at 41.1 eV. The principal W 4f features located at 35.5 and 37.6 eV account for 84% of W 4f signals while indicating W is 6+ oxidation state. The remaining 16 percent of the peaks are assigned to the 4f7/2 and 4f5/2 doublet signatures of W in 5+ oxidation state which appear at 36.4 and 34.3 eV. The XPS data excludes WO2 and metallic tungsten or 4 + oxidation states because the spectrum shows no doublets at 33.3 eV and 35.5 eV and 31.2 and 33.4 eV peaks [110]. Undoubtedly, these observations on the various chemical states of the elements in the CuO@HEAG@rGO hybrid nanostructure represent a highly successful formation of this hybrid nanostructure.

(a) (b)

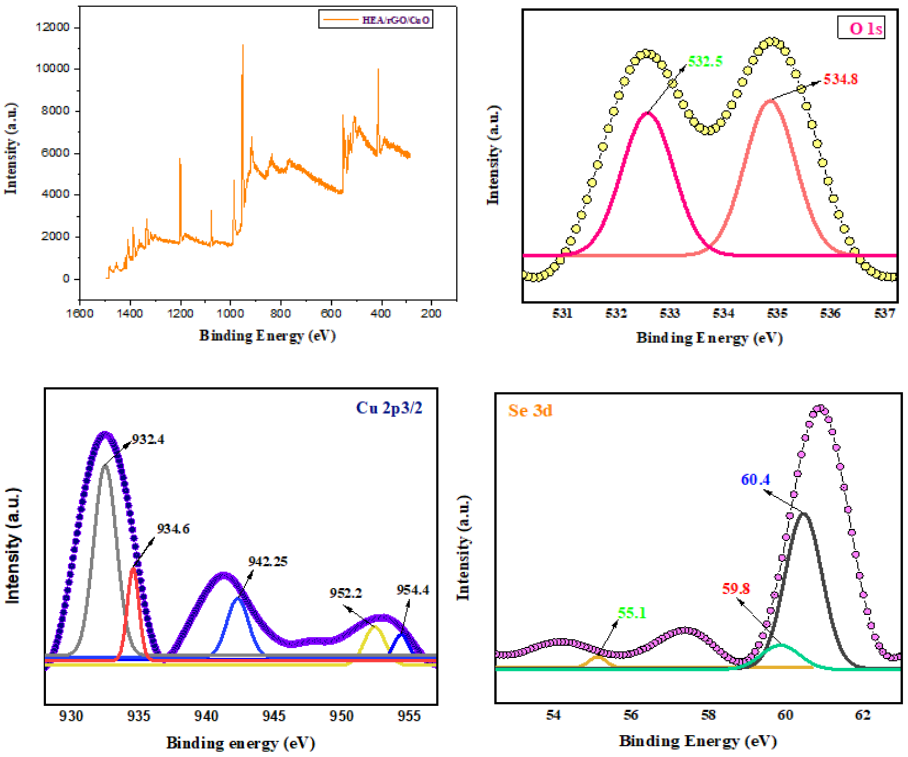

(c) (d)

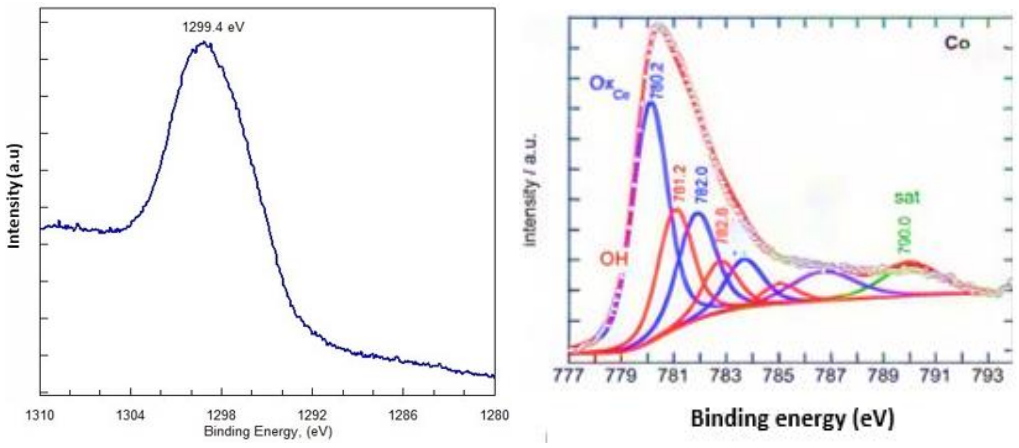

(e) (f)

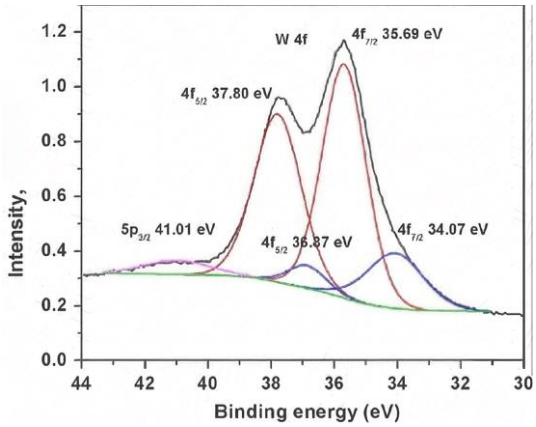

(g)

Figure 4.5: XPS Graphs a, b, c, d, e, f, and g show elemental composition and oxidation states of Cu, Se, O, C, Mo, Co, W.

4.6 X-ray Diffraction Spectroscopy

X-ray diffraction (XRD) is a non-destructive analytical method commonly used to identify phases and analyze the structural properties of crystals. Copper crystallizes into a face-centered cubic (FCC) form. Cu Kα radiation produces XRD peaks at 43.3°, 50.4°, and 74.1° 2θ, corresponding to the (111), (200), and (220) planes. These peaks serve as phase identification fingerprints, which are then compared to conventional data [111]. Cobalt may occur in two structures: hexagonal close-packed (HCP) and face-centered cubic (FCC), with the former being more stable at ambient temperature. The primary XRD peaks for HCP cobalt are seen at 44.2°, 47.5°, and 75.9° 2θ. Because of potential polymorphism, phase identification

necessitates a comparison with reference patterns [112]. Zinc's structure is hexagonal close-packed (HCP). The main XRD peaks are at 36.3°, 39.1°, and 43.3° 2θ, representing the (100), (002), and (101) planes, respectively. These peaks are used to check the zinc samples' phase and purity [113]. Tungsten crystallizes in a body-centered cubic (BCC) form. The XRD pattern reveals significant reflections at 40.3°, 58.3°, and 73.1° 2θ, which correspond to the (110), (200), and (211) planes. To determine the phase, the pattern is compared to standard data [114]. Molybdenum has a BCC structure with prominent peaks at 40.5°, 58.6°, and 73.3° 2θ. To differentiate between the two due to their similarities to tungsten, rigorous study and comparison with reference patterns are required [115]. Selenium often crystallizes in a trigonal (hexagonal) form. The XRD pattern shows peaks at 23.5°, 29.3°, and 43.5° 2θ, indicative of the trigonal allotrope. These peaks are necessary for phase verification [116]. The obtained XRD pattern for each element was examined by measuring the peak intensities and d-spacing. These were then compared to established standards in the ICDD database, usually utilizing the three strongest lines (d1, d2, and d3) to determine the phase. This method guarantees accurate phase identification even when numerous compounds have comparable d-values.

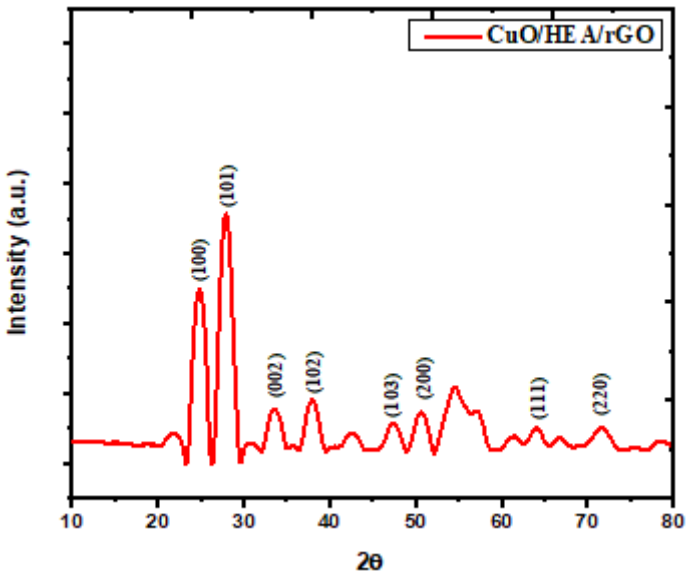

Figure 4.6: XRD pattern showing the characteristic diffraction peaks of the analyzed samples

4.7 Gas Chromatography

Gas Chromatography was done to identify and quantify methanol in the HEAG and composite CuO-HEAG@rGO.

Methanol Analysis via Gas Chromatography (GC)

1. Standard Methanol Data

Across several injections, the standard methanol sample's retention time (RT) remained consistent at 12.81 minutes. The region of the peak for the standard ranged between 267,688.05-268,053.45, demonstrating the GC instrument's reliability and repeatability in identifying methanol. The uniformity of the peaks and a tailing coefficient that ranges roughly 0.64-0.68 help confirm the standard data's validity. This standard information was utilized to determine and evaluate the prepared samples' GC data [117].

The RTs for HEAG and CuO-HEAG@rGO were similar to the reference methanol sample, showing that the identified chemical was methanol. However, the peak amplitude was substantially smaller than the standard, indicating a much lower methanol content in the sample. This may be measured using the curve for calibration generated by the standard.

Comparison and Implications.

Percentage Trends: HEAG contains a low percentage of methanol (3.45%), whereas CuO-HEAG@rGO contains a greater quantity (9.77%).

Retention Times: Both samples had RTs near to the standard, confirming methanol identification.

Peak Quality: Both samples had satisfactory peak symmetry, suggesting that the GC apparatus was performing properly.

(A)

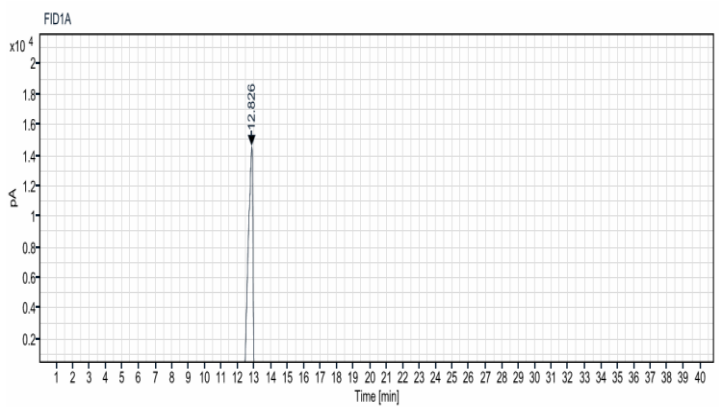

(b)

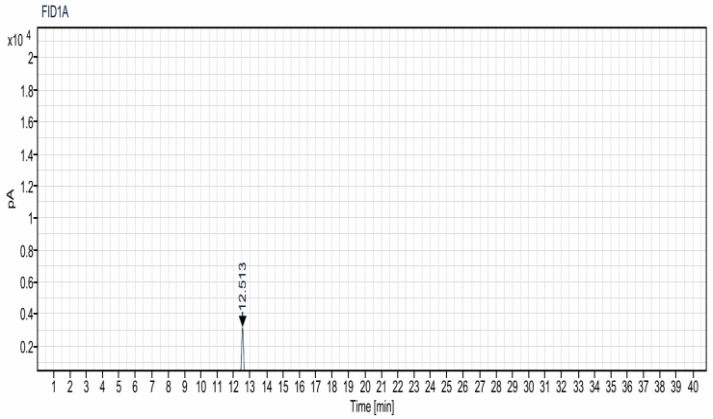

(c)

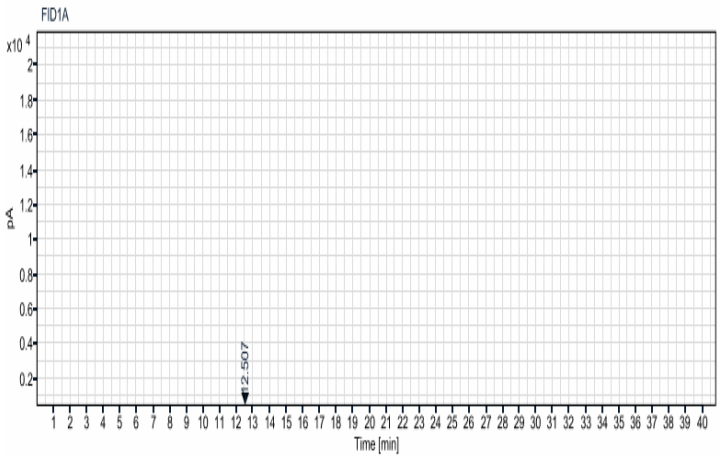

Figure 4.3: (a)GC methanol standard data chromatogram vs (b) Methanol chromatogram of HEAG (c) Methanol chromatogram of CuO-HEAG@rGO

Table 1: GCFID signals data

Sample name	Retention time	Peak Area Percent	Tailing Factor
Methanol	**12.826**	**100**	**0.67832**
HEAG	**12.507**	**100**	**1.16209**
CuO-HEAG@rGO	**12.513**	**100**	**0.95505**

4.8 Photocatalytic CO_2 Reduction into Methanol

The photoreduction activity on HEAG ($ZnCl_2$, $CoCl_2$, Na_2SeO_3, Na_2WO_4, $(NH_4)6Mo_7O_{24}$) and HEAG@CuO@rGO samples was exposure to visible and UV light. The maximum methanol output of HEAG@CuO@rGO nanocomposites was greater than that of the high entropy aerogel without the co-catalyst, as shown in Figure and Table . When HEAG is compared to the co-catalyst-based HEAG@CuO@rGO, it is shown that the ternary systems based on CuO and reduced graphene oxide significantly enhance catalytic capabilities, indicating a close bond between graphene and the linked semiconductor components. Additionally, the good interfacial contact between HEAG and reduced graphene oxide nanosheets is demonstrated by HEAG aided by CuO. After six hours of testing the HEAG-CuO-rGO composites' photocatalytic activity under UV (k > 100) and visible (k > 100) light irradiation, the methanol production that resulted is displayed in the Figure, the photocatalytic activity for methanol production was determined by plotting methanol yield as a function of time for GO, CuO@rGO, HEAG (1 & 6 hours), HEAG-CuO-rGO (1 & 6 hours), under visible light. The rate of methanol yield was calculated by utilizing this formula:

$$\boldsymbol{Yield} = \frac{\boldsymbol{Conc.\ of\ methanol\ (ppm)} \times \boldsymbol{Volume\ of\ solution\ (l)}}{\boldsymbol{Mass\ of\ catalyst\ (g)} \times \boldsymbol{Reaction\ time\ (hour)}}$$

The quantum efficiency or yield can be estimated by using this expression

$$\boldsymbol{QE} = \frac{\boldsymbol{no.of\ moles\ of\ product\ formed} \times \boldsymbol{no\ of\ moles\ of\ e^{-1}\ required}}{\boldsymbol{no.of\ photon\ absorbed\ by\ photocatalyst}} \times \mathbf{100}$$

$$QE = \frac{\text{no. of moles } \left(\frac{mol}{l}\right) \times 6 \times N_A}{IE \times A \times \lambda \times T \times Hc}$$

In this equation, IE represents light intensity (3.5729 w/cm2), A represents photocatalyst irradiation (0.00321 m2), λ represents light wavelength (>400nm for visible light), h represents plank's constant (6.64 * 10-34), C represents light speed (3* 10-8ms-1), T represents reaction time in seconds (3600s), and NA represents Avogadro's number (6.022 * 1023) [118]. The selectivity of the photocatalyst for a particular product can be enumerated from the given expression

Table 2. Comparison of Yield

Samples	**Precursor**	**Agent**	**Light (nm)**	**Rx Time (h)**	**Methanol production (µmol $g^{-1}h^{-1}$) during 1st hour**	**Methanol production (µmol $g^{-1}h^{-1}$) during 6th hour**	**Quantum Efficiency (%)**
GO	**CO_2**	**H_2O**	**400/265**	**6**		———	———
HEAG	**CO_2**	**H_2O**	**400/265**	**6**	**700.72**	**267.94**	**0.236**
HEAG@CuO@rGO	**CO_2**	**H_2O**	**400/265**	**6**	**1400.34**	**1143.3**	**1.13**

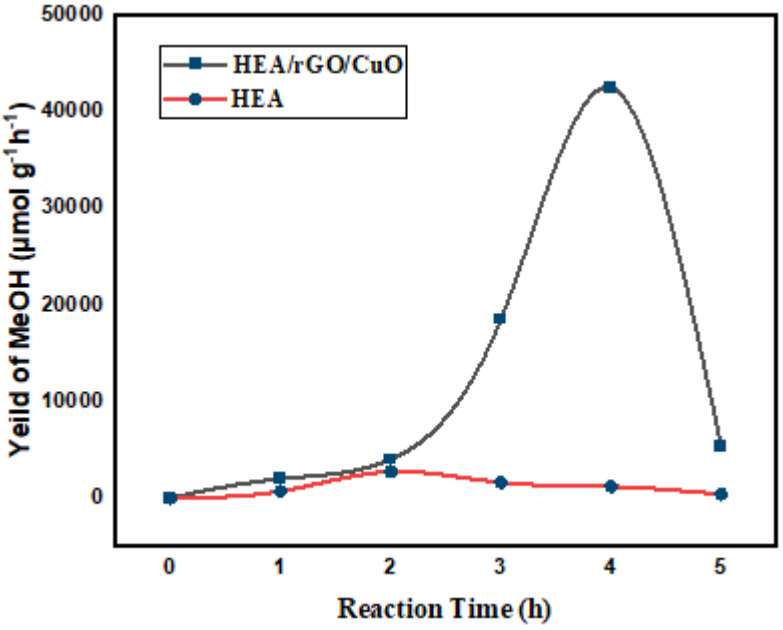

Figure 4.8.: Methanol yield of HEAG and HEAG@CuO@rGO

The effect of CuO loading on HEAG-doped reduced graphene oxide is depicted in the figure. The yield of methanol, along with the quantum efficiency, decreases from having CuO@rGO@HEAG to not having CuO@rGO@HEAG. Consequently, the calculated amount of methanol also decreases. A higher dispersion of 2D graphene on CuO nanoparticles allows for maximal adsorption of visible light-mediated electron transitions to the conduction band of copper oxide, resulting in increased light absorption. This, along with a larger number of oxygen vacancies and Schottky defects, supports photo-mediated electron transfer and reduces carrier charge recombination. These factors contribute to a greater electron acceptance from the graphene framework, which lowers the probability of charge recombination (e+, h) [119]. A significant interfacial synergistic effect between HEAG and CuO is facilitated by CuO supporting the interaction between HEAG and rGO, leading to enhanced formation of heterojunctions. The HEAG configuration at 6 hours (2.679 mmol g^{-1} h^{-1}) was found to exhibit photocatalytic activity comparable to that of HEAG@CuO@Rgo at the 1st hour (1.40 mmol$g^{-1}h^{-1}$) being less than HEAG@CuO@rGO (1.143 mmol g^{-1} h^{-1}) at 6 hours.

4.8.1. Photo-electric performance analysis

The key to effective photocatalytic photoreduction of carbon dioxide is the separation efficiency of the charge carrier produced by photocatalysis in the photocatalyst. We anticipated excellent photocatalyst performance due to the increased charge separation. Photoluminescence PL at room temperature was used to test the photocatalyst's separation efficiency. The enhanced intensity of the ternary composite made from copper oxide-doped HEAG and reduced graphene oxide can be attributed to the heterojunction interface between CuO and HAEG, as well as the surface defects present in rGO. This suggests that the efficiency of photo-generated carrier transfer at the 1D-2D-3D interface is significantly greater than that of other samples. The exceptional performance of CuO-HEAG@rGO in CO_2 photoreduction is linked to its favorable photoelectric properties.

CHAPTER 5

DISCUSSION

The use of high-entropy aerogel photocatalysts with co-catalysts of copper oxide (CuO) and reduced Graphene oxide (rGO) has demonstrated significant improvements towards photocatalytic levels of CO_2 reduction to methanol. The two work together to change structural and electrical parameters, which make activity better and more selective.

SEM inspection reveals that the aerogel's hierarchical porous structure has a large surface area (BET results) and a significant number of active sites for CO_2 adsorption and activation. FTIR spectra showed the existence of functional group (C=O and Cu-O) required for stabilizing chemical intermediates. XPS measurements verified the presence of Cu^{+}/Cu^{2+} species and the promoting electron transfer and inhibiting charge recombination by adding rGO. The bandgap of 1.5 eV (UV-Vis study) calculated from the lower bandgap is obtained due to the small bandgap of CuO and the conductive network of rGO. By using visible light, the optimized CuO/rGO modified aerogel surpassed many documented systems (e.g., $Ni/InTaO_4$, at ~ 6 $\mu mol \cdot g^{-1} \cdot h^{-1}1$) and achieved methanol production of 1143.2 $\mu mol \cdot g^{-1} \cdot h^{-1}$. This improvement has a reason for: Charge separation: rGO serves as an electron sink and directs electrons to the CuO active sites for CO_2 reduction and prolongs carrier lifetimes. Intermediate Stabilization: CuO has been shown to stabilize the *OCHO intermediate, aiding the selectivity towards methanol rather than competing products such as HCOOH2 or CO. Band Structure Modulation: First aligned redox potentials for the reduction of CO_2 to methanol and preserving the ability to oxidize water, a 1.5 eV bandgap retained.

The remarkable preservation of more than 90% activity over five cycles was attributed to rGO's protective role in avoiding CuO oxidation or agglomeration, with no rGO limitation: the macroporous structure ensures reactant diffusion and light penetration.

The methanol production rate for this aerogel is competitive to Cu/ZnO_x@MOF systems (2.59 g MeOH kg^{-1} h^{-1}), and with the further advantage of simpler synthesis and lower cost. The compositional complexity of the high entropy framework is

probably suppressing the deactivation pathways, but more research is needed to identify which individual constituent is responsible of each possible deactivation pathway.

This system can work but more study is required to assess its scalability and industrial stability. Methanol selectivity can be tuned to further by varying CuO/rGO ratios, as well as, examining dopant (like transition metals). When implementing in conjunction with renewable energy, bulky CO_2 valorization may become more sustainable.

This work demonstrates how high-entropy aerogels and carefully selected co-catalysts can bridge the gap between cutting-edge laboratory-scale procedures and practical photocatalytic applications.

CONCLUSIONS

This work shows that a high entropy aerogel photocatalyst with CuO and rGO as cocatalysts achieves excellent efficiency in reducing CO_2 to methanol under visible light. This hierarchical porous CuO/rGO modified aerogel demonstrated a methanol yield of 1143.2 μmol $g^{-1}h^{-1}$ that outperformed state-of-the-art photocatalysts having a tailored bandgap (1.5 eV, UV-VIS).

High surface area and compositional flexibility of the high-entropy aerogel framework were provided for stabilizing active sites. Through the chemisorption of beneficial CuO nanoparticles and their use in facilitating activation and *OCHO intermediate binding, the selectivity is steered towards methanol; however, the activity retention is also enhanced by rGO by providing a protection matrix, enabling long-term stability (> 90% activity retention over five cycles). FTIR, XPS, and XRD combined characterization, and band alignment analysis suggested charge transfer balance between redox potentials for CO_2 reduction (to methanol) and water oxidation in CuO/rGO system favors TypeII-scheme charge transfer.

Solutions to problems of light penetration and mass transport are achieved by the macroscale aerogel structure, which is also scalable relative to powdered catalysts.

For practical implementation, scaling reactor designs and incorporating renewable energy sources (like solar concentrators) will be essential. This work bridges the gap between basic research and sustainable fuel production by advancing high-entropy aerogels as a flexible platform for solar-driven CO_2 valorization.

REFERENCES

1. A.A. Mehrizi, M. Farhadi, K.Sedighi, M.A. Delavar. Effect of fin position and porosity onheat transfer improvement in a plate porous media heat exchanger, *J Taiwan Inst. Chem. Eng*. **2013**, 44, 420-431.
2. A.Y Al-Maharma, S.P. Patil B. Markert, Effects of porosity on the mechanical properties ofadditively manufactured components: a critical review, *Mater. Res. Express*, **2020**, 7, 122001.
3. A. Thomas, Much ado about nothing a decade of porous materials research, *Nat. Commun*. **2020**, 11, 4985.
4. H. Zhou, H. Li, A. Abdelhady, X. Liang, H. Wang, B. Yang, Experimental investigation on the effect of pore characteristics on clogging risk of pervious concrete based on CT scanning,*Constr. Build. Mater*. **2019**, 212, 130-139.
5. Bo. Zdravkov, J. Čermák, M. Šefara, J. Janků, Pore classification in the characterization ofporous materials: A perspective, *Cent. Eur. J. Chem*. **2007**, 5, 385-395.
6. J. Rouquerol, D. Avnir, C. W. Fairbridge, D. H. Everett, J. M. Haynes, N. Pernicone, J. D.F. Ramsay, K. S. W. Sing and K. K. Unger, Recommendations for the characterization of porous solids (Technical Report), *Pure Appl. Chem.* **2009**, 66, 1739-1758.
7. T. Zhu1, Y. Han, S. Liu, B. Yuan, Y. Liu, H. Ma, Porous materials confining single atoms for catalysis, *Front. Chem*. **2021**, 9, 717201.
8. X. Fan, Y. Jiao, Chapter 5 - Porous materials for catalysis: toward sustainable synthesis andapplications of zeolites, *Sustain. Nanoscale Eng.* Elsevier Inc. (**2019**), 115-137.
9. Y. Li, Y. Fu, C. Lai, L. Qin, B. Li, S. Liu, H. Yi, F. Xu, L. Li, M. Zhang, M. Xu, C. Duc,W. Chen, Porous materials confining noble metals for the catalytic reduction of nitroaromatics:controllable synthesis and enhanced mechanism, *Environ. Sci.: Nano*. **2021**, 8, 3067-3097.
10. M. Mungmart, U. Kijsirichareonchai, N. Tonanon, S. Prechanont, J. Panpranot, T. Yamamoto, A. Eiadua, N. Sano, W. Tanthapanichakoon, T. Charinpanitkula, Metal catalysts impregnated on porous media for aqueous phenol decomposition within three-phase fluidized-bed reactor, *J. Hazard. Mater.* **2011**, 185, 606-612.
11. G.S. Day, H.F. Drake, H.C. Zhou, M.R. Ryder, Evolution of porous materials from ancientremedies to modern frameworks, *Commun. Chem.* **2021**, 4, 114.
12. A. Zanoletti, F. Bilo, L. Borgese, L.E. Depero, A. Fahimi, J. Ponti, A. Valsesia, R. La Spina, T. Montini, E. Bontempi, SUNSPACE, A porous material to reduce air particulate matter(PM), *Front. Chem.* **2018**, 6, 534.
13. H.K. Patel, R.K. Kalaria, M.R. Khimani, 20 - Nanotechnology: A promising tool for Bioremediation, *Removal of toxic pollutants through microbiological and tertiary treatment*, Elsevier Inc. (**2020**), 515-547.
14. O.W. Florke, H.A. Graetsch, F. Brunk, L. Benda, S. Paschen, H.E. Bergna, W.O. Roberts,W.A. Welsh, C. Libanati, M. Ettlinger, Silica, *Ullmann's Encyclopedia of Industrial Chemistry*.in Wiley-VCH Verlag, John Wiley & Sons, Ltd. (**2008**).

15. C.M. Wang, W.S. Liao, Designing sensing devices using porous composite materials, *J. Compos. Sci*. **2021**, 5, 35.
16. Y. Liu, Y. Zhai, Y. Xia, W. Li, D. Zhao, Recent Progress of porous materials in lithium- metal Batteries, *Small Struct.* **2021**, 2, 2000118.
17. Z. Chen, K.O. Kirlikovali, K.B. Idrees, M.C. Wasson, O.K. Farha, Porous materials for hydrogen storage, *Chem* **2022**, 8, 693-716.
18. T.W. Clyne, I.O. Golosnoy, J.C. Tan, A.E. Markaki, Porous materials for thermalmanagement under extreme conditions, *Phil. Trans. R. Soc. A* **2006,** 364, 125–146.
19. S. Rashidi, M.H. Kashefi, K.C. Kim, O. Samimi-Abianeh, Potentials of porous materials for energy management in heat exchangers – A comprehensive review, *Appl. Energy* **2019**, 243,203-232.
20. F. Anjum, M.Y. Naz, A. Ghaffar, K. Kamran, S. Shukrullah, S. Ullah, Sustainable insulating porous building materials for energy-saving perspective: Stones to environmentally friendly bricks, *Constr. Build. Mater*. **2022**, 318, 125930.
21. M. Quintard, Introduction to heat and mass transport in porous media, *Porous media in high temperature and high speed flows*, "STO-EN-AVT-261" North Atlantic Treaty Organization (NATO) (**2016**).
22. D. Křemenáková, J. Militký, M. Venkataraman, R. Mishra, Thermal insulation and porosity-from macro- to nanoscale, *Thermal Physics and Thermal Analysis*, Springer (**1965**), 425-448.
23. L. Cao, Q. Fu, Y. Si, B. Ding, J. Yu, Porous materials for sound absorption, *Compos. Commun.* **2018**, 10, 25-35.
24. P. Yang, T. Zhou, D. Jia, Z. Qin, Y. Wu and H. Bai, Compressive mechanical behavior and model of composite elastic-porous metal materials, *Mater. Res. Express* **2021**, 8, 126518.
25. A.A. Mahmoud, M. Abd-Elbasseer, Characterization of poly-isoprene rubber layer backedwith porous material as sound absorber and vibration damper, *J. Am. Sci.* **2011**, 7, 102-109.
26. J.L. Hernandez, K.A. Woodrow, Medical Applications of Porous Biomaterials: Features of Porosity and Tissue-Specific Implications for Biocompatibility, *Adv. Healthcare Mater*. **2022**, 11, 2102087.
27. G. Ahuja, K. Pathak, Porous carriers for controlled/modulated drug delivery, *Indian J Pharm Sci*. **2009,** 71, 599-607.
28. S. Rojas, T. Devic, P. Horcajada, Metal organic frameworks based on bioactive components, *J. Mater. Chem. B* **2017**, 5, 2560-2573.
29. F. Matassi, A. Botti, L. Sirleo, C. Carulli, M. Innocenti, *Clin. Cases Miner. Bone Metab.* **2013**, 10, 111-115.
30. C.L. Perez, F.P. Casciatori, J.C. Thoméo, Improving enzyme production by solid-state cultivation in packed-bed bioreactors by changing bed porosity and airflow distribution,*Bioprocess. Biosyst. Eng.* **2021**, 44, 537-548.
31. S. Park, G. Stephanopoulos, Packed bed bioreactor with porous ceramic beads for animalcell culture, *Biotechnol Bioeng*. **1993,** 41, 25-34.
32. IUPAC. Compendium of Chemical Terminology, 2nd ed. (the "Gold Book"). Compiled by A. D. McNaught and A. Wilkinson. Blackwell Scientific Publications, (**1997**).

33. J.P. Vareda, A. Lamy-Mendes, L. Durães, A reconsideration on the definition of the termaerogel based on current drying trends, *Microp. Mesoporous Mater*. **2018**, 258, 211-216.
34. C. Ziegler, A. Wolf, W. Liu, A.K. Herrmann, N. Gaponik, A. Eychmüller, Modern Inorganic Aerogels, *Angew. Chem. Int. Ed*. **2017**, 56, 13200-13221.
35. M. Bertino, M.A. Aegerter, N. Leventis, M.M. Koebel, Aerogels Handbook, *Adv. Sol-GelDeriv. Materials Technol.*, Spinger (**2011**).
36. D.A. Loy, Sol–Gel Processing, *Encyclopedia of Physical Science and Technology (Third Edition)*, Elsevier Inc. (**2003**), 257-276.
37. N. Job, A. Théry, R. Pirard, J. Marien, L. Kocon, J.-N. Rouzaud, F. Béguin, J.-P. Pirard, Carbon aerogels, cryogels and xerogels: Influence of the drying method on the texturalproperties of porous carbon materials, *Carbon* **2005**, 43, 2481–2494.
38. B. Denoulet, How to effectively use organic solvents in lyophilization, "https://www.barts- blog.net/how-to-effectively-use-organic-solvents-in-lyophilization" 2020. (Accessed June 2022).
39. V. Baudron, P. Gurikov, I. Smirnova, S. Whitehouse, Porous Starch Materials viaSupercritical- and Freeze-Drying, *Gels* **2019**, 5, 12.
40. S.S. Kistler, Coherent Expanded Aerogels and Jellies, *Nature*, **1931**, 127, 741.
41. S. Zhang, D. Zhao, Aerospace Materials Handbook, *Advances in Materials Science and Engineering*, CRC Press (**2012**).
42. C.A. García-González, M. Alnaief, I. Smirnova, Polysaccharide-based aerogels— Promising biodegradable carriers for drug delivery systems, *Carbohydr. Polym*. **2011**, 86, 1425-1438.
43. W.S. Hummers, R.E. Offeman, Preparation of graphitic oxide, *J. Am. Chem. Soc*. **1958**, 80, 1339.A. Du, B. Zhou, Z. Zhang, J. Shen, A Special Material or a New State of Matter: A Reviewand Reconsideration of the Aerogel, *Materials* **2013**, 6, 941-968.
44. T. Woignier, J. Primera, A. Alaoui, F. Despetis, S. Calas-Etienne, A. Faivre, L. Duffours, C. Levelut, P. Etienne, Techniques for characterizing the mechanical properties of aerogels, *J.Sol-Gel Sci. Technol.* **2020**, 93, 6-27.
45. L. Dou, X. Zhang, X. Cheng, Z. Ma, X. Wang, Y. Si, J. Yu, B. Ding, Hierarchical Cellular structured ceramic nanofibrous aerogels with temperature-invariant superelasticity for thermalinsulation, *ACS Appl. Mater. Interfaces* **2019**, 11, 29056–29064.
46. NASA, Polymer Cross-Linked Aerogels (X-Aerogels), "https://technology.nasa.gov/ patent/LEW-TOPS-20" (Accessed May 2022).
47. C. Dixon, "https://www.nytimes.com/2004/01/20/science/using-the-right-bait-to-catch-a-comet.html", New York Times, (Accessed May 2022).
48. N.B. Andersen, L. Olsen, Super-insulated windows with silica aerogel, Energy Conservation in Buildings, *The Achievement of 50% Energy Saving: An Environmental Challenge*, Elsevier Inc. (**1991**), 119-124.
49. C.H. Yu, Q.J. Fu, S.C.E. Tsang, 13 - Aerogel materials for insulation in buildings, *Materials for energy efficiency and thermal comfort in buildings*, Woodhead Publishing (**2010**),319-344.
50. NASA, Rover Temperature Controls, "https://mars.nasa.gov/mer/mission/rover/temperature/#aerogel", (Accessed May 2022).

51. Aerogel Technologies, About Airloy® Ultramaterials, “http://www.aerogeltechnologies.com/airloy/about-airloy-ultramaterials/”, (Accessed June2022).
52. C.A. García-González, A. Sosnik, J. Kalmár, I. De Marco, C. Erkey, A. Concheiro, C. Alvarez-Lorenzo, Aerogels in drug delivery: From design to application, *J. Control. Release* **2021**, 332, 40-63.
53. S. Yu, S. Song, R. Li, B. Fang, The lightest solid meets the lightest gas: an overview of carbon aerogels and their composites for hydrogen related applications, *Nanoscale* **2020**,12, 19536-19556.
54. Q.B. Thai, D.K. Le, N.H.N. Do, P.K. Le, N. Phan-Thien, C.Y. Wee, H.M. Duong, Advanced aerogels from waste tire fibers for oil spill-cleaning applications, *J. Environ. Chem.Eng*. **2020**, 8, 104016.
55. M.A. Iskandar, E.B. Yahya, H.P.S.A. Khalil, A.A. Rahman, M. A. Ismail, Recent progressin modification strategies of nanocellulose-based aerogels for oil absorption application,*Polymers* **2022**, 14, 849.
56. J. Choi, D.J. Suh, Catalytic Applications of Aerogels, *Catal. Surv. Asia* **2007**, 11, 123-133.
57. H. Gunes, Y. Özbakir, S.B. Barim, H. Yousefzadeh, S.E. Bozbag, C. Erkey, A remarkable class of nanocomposites: aerogel supported bimetallic nanoparticles, *Front. Mater*. **2020**, 7, 18.
58. D.J. Suh, T.-J. Park, H.-Y. Han, J.-C. Lim, Synthesis of high-surface-area zirconia aerogels with a well-developed mesoporous texture using CO_2 supercritical drying, *Chem. Mater*. **2002**,14, 1452–1454.
59. M. Kubovics, A. Trigo, A. Sánchez, G. Marbán, A. Borrás, J. Moral-Vico, A.M. López- Periago, C. Domingo, Role of graphene oxide aerogel support on the CuZnO catalytic activity: enhancing methanol selectivity in the hydrogenation reaction of CO_2, *Chem. Cat. Chem.* **2022**,e202200607.
60. X.-R. Gao, Z. Xing, Z.-J. Li, X.-Y. Dong, Z.-C. Ju, C.-L. Guo, A review on recent advancesin carbon aerogels: their preparation and use in alkali-metal ion batteries, *New Carbon Mater*. **2020**, 35, 486-507.
61. Y. Lv, L. Ding, X. Wu, N. Guo, J. Guo, S. Hou, F. Tong, D. Jia, H. Zhang, Coal-based 3Dhierarchical porous carbon aerogels for high performance and super-long life supercapacitors, *Sci. Rep*. **2020**, 10, 7022.
62. M.J. Burchell, G. Graham, A. Kearsley, Cosmic dust collection in aerogel, *Annu. Rev.Earth Planet. Sci.* **2006**, 34, 385-418.
63. A. Whalen (2005), Catching comet dust “*https://solarsystem.nasa.gov/ stardust/tech/aerogel.html”* (Accessed May 2022).
64. S.J. McNeil, H. Gupta, Emerging applications of aerogels in textiles, *Polym. Test*. **2022**,106, 107426.
65. R. Gupta, J.-J. Shim, *Solubility in supercritical carbon dioxide*, CRC Press (**2006**).
66. S.G. Kazarian, M.F. Vincent, F.V. Bright, C.L. Liotta, C.A. Eckert, Specific Intermolecular Interaction of Carbon Dioxide with Polymers, *J. Am. Chem. Soc.* **1996**, 118, 1729-1736.
67. K.H. Kim, Y. Kim, Theoretical studies for the supercritical CO_2 solubility of organophosphorous molecules: lewis acid-base interactions and C-H···O weak hydrogen bonding, *Bull. Korean Chem. Soc.* **2007**, 28, 2454,2458.

68. P.N. Khanh, N.T. Trung, Understanding interaction capacity of CO_2 with organiccompounds at molecular level: a theoretical approach, *Carbon dioxide chemistry, capture andoil recovery*, IntechOpen, (**2018**).
69. D.S. Bulgarevich, T. Sako, T. Sugeta, K. Otake, M. Sato, M. Uesugi. Masahiro Kato, Solvent Polarities of Supercritical CO_2/Methanol Mixtures, *Rev. High Pressure Sci. Technol*. **1998**, 7, 1423-1425.
70. Zhu H, Zhu Z, Hao J, Sun S, Lu S, Wang C, et al. High-entropy alloy stabilized active Ir for highly efficient acidic oxygen evolution. Chemical Engineering Journal. 2022;431:133251.
71. Ju Y, Zhang A, Xu Z, Liu Y, Zhu X, Zhu P, et al. Formicary-like PtBi1.5Ni0.2Co0.2Cu0.2 high-entropy alloy aerogels as an efficient and stable electrocatalyst for methanol oxidation reaction. Chemical Engineering Journal. 2023;473:145347.
72. Liu H, Qin H, Kang J, Ma L, Chen G, Huang Q, et al. A freestanding nanoporous NiCoFeMoMn high-entropy alloy as an efficient electrocatalyst for rapid water splitting. Chemical Engineering Journal. 2022;435:134898.
73. Li H, Huang HH, Chen Y, Lai F, Fu HC, Zhang H, et al. High-Entropy Alloy Aerogels: A New Platform for Carbon Dioxide Reduction. Advanced Materials. 2022 Nov 14;35:2209242.
74. Nie N, Zhang Y, Gu Y, Du H, Yuan Y, Yang Y, et al. Chelating Co-reduction Strategy for the Synthesis of High-Entropy Alloy Aerogels. Inorganic Chemistry. 2023 Jul 25;62(31):12337–44
75. Fu S, Liu D, Deng Y, Li M, Zhao H, Guo J, et al. Medium-entropy ceramic aerogels for robust thermal sealing. Journal of materials chemistry A, Materials for energy and sustainability. 2023 Jan 1;11(2):742–52.
76. Sakthisabarimoorthi A, Ayman MT, Ryu S, Yoon D. Synthesis of hollow AlN microsphere by hydrothermal and carbothermal reduction–nitridation hybrid technique. Ceramics International. 2024 Jun 1;
77. Kaleva A, Heinonen S, Nikkanen JP, Levänen E. Synthesis and crystallization of titanium dioxide in supercritical carbon dioxide (scCO2). 2017 Feb 1;175(1):012034
78. Zhang Shibiao, Zhang X, Zhang J, Zheng H, Li G, Zeng K, et al. Three-dimension in-situ nitrogen doping porous cellulosic biomass-based carbon aerogel for electrocatalytic CO2 reduction. Fuel Processing Technology 2023;242:107612.
79. Jiang, X., Kong, Y., Zhao, Z., & Shen, X. (2020). Spherical amine grafted silica aerogels for CO2 capture. *RSC Advances*, *10*(43), 25911–25917.
80. Dong, Z., Peydayesh, M., Donat, F., Jin, T., Müller, C. R., & Mezzenga, R. (2023). Amine-Functionalized Amyloid Aerogels for CO2 Capture. *Chemsuschem*, e202300767
81. Yao R, Yao Z, Zhou J. Microstructure, thermal and electrical properties of polyaniline/phenolic composite aerogel. Journal of Porous Materials. 2018 Apr;25:495-501.
82. Bernier JV, Suter RM, Rollett AD, Almer JD. High-energy X-ray diffraction microscopy in materials science. Annual Review of Materials Research. 2020 Jul 1;50(1):395-436

83. Shi Y, Wang Y, Li S, Li R, Cui Y, Wang YD. Recrystallization Texture Analysis of FeCoNiCrMnAl0. 5 High-Entropy Alloy Investigated by High-Energy X-ray Diffraction. Metals. 2022 Oct 6;12(10):1674
84. Brechtl J, Lee C, Liaw PK. High-entropy materials: fundamentals and applications. Journal of Materials Research and Technology. 2023 Mar 1;23(1).
85. Li C, Xue Y, Hua M, Cao T, Ma L, Wang L. Microstructure and mechanical properties of AlxSi0. 2CrFeCoNiCu1− x high-entropy alloys. Materials & Design. 2016 Jan 15;90:601-9.
86. Górecki K, Bała P, Cios G, Stępień M, Kozieł T, Wieczerzak K, Tokarski T. X-ray diffraction and EBSD study of Al-Ti-Co-Ni-Fe high-entropy alloy. Acta Physica Polonica A. 2016 Oct;130(4):991-2.-
87. Górecki K, Bała P, Cios G, Stępień M, Kozieł T, Wieczerzak K, Tokarski T. X-ray diffraction and EBSD study of Al-Ti-Co-Ni-Fe high-entropy alloy. Acta Physica Polonica A. 2016 Oct;130(4):991-2.
88. Fan L, Ji Y, Wang G, Chen J, Chen K, Liu X, Wen Z. High entropy alloy electrocatalytic electrode toward alkaline glycerol valorization coupling with acidic hydrogen production. Journal of the American Chemical Society. 2022 Apr 11;144(16):7224-35.
89. Xue Y, Zhao X, An Y, Wang Y, Gao M, Zhou H, Chen J. High-entropy (La0. 2Nd0. 2Sm0. 2Eu0. 2Gd0. 2) 2Ce2O7: A potential thermal barrier material with improved thermo-physical properties. Journal of Advanced Ceramics. 2022 Apr;11(4):615-28.
90. Asim M, Hussain A, Khan S, Arshad J, Butt TM, Hana A, Munawar M, Saira F, Rani M, Mahmood A, Janjua NK. Sol-gel synthesized high entropy metal oxides as high-performance catalysts for electrochemical water oxidation. Molecules. 2022 Sep 13;27(18):5951.
91. Yang G, Luo H, Ohba T, Kanoh H. CO2 capture by carbon aerogel–potassium carbonate nanocomposites. International Journal of Chemical Engineering. 2016;2016(1):4012967.
92. Ello AS, Yapo JA, Trokourey A. N-doped carbon aerogels for carbon dioxide (CO2) capture. Afr. J. Pure Appl. Chem. 2013 Feb;7(2):61-6.
93. Abdelhafiz A, Wang B, Harutyunyan AR, Li J. Carbothermal shock synthesis of high entropy oxide catalysts: dynamic structural and chemical reconstruction boosting the catalytic activity and stability toward oxygen evolution reaction. Advanced Energy Materials. 2022 Sep;12(35):2200742
94. Gubicza J, Heczel A, Lilensten L, Couzinié JP, Perrière L, Guillot I, Hocini A. Microstructural investigation of plastically deformed Ti {sub 20} Zr {sub 20} Hf {sub 20} Nb {sub 20} Ta {sub 20} high entropy alloy by X-ray diffraction and transmission electron microscopy. Materials Characterization. 2015 Oct 15;108.
95. Liu X, Su C, Zhong Y, Zhu X, Wu Z, Cui S. High entropy (LaCeSmEuNd) 2Zr2O7 ceramic aerogel with low thermal conductivity and excellent structural heat resistance. Journal of the European Ceramic Society. 2022 Oct 1;42(13):5964-72.

96. Shandurkov D, Danchova N, Spassov T, Petrov V, Gutzov S. Luminescence of Binary-Doped Silica Aerogel Powders: A Two-Step Sol-Gel Approach. Gels. 2024;10(2):104.
97. Tang Y, Lai Y, Gao R, Chen Y, Xiong K, Ye J, et al. Functional Aerogels Composed of Regenerated Cellulose and Tungsten Oxide for UV Detection and Seawater Desalination. Gels. 2022;9(1).
98. Fuente, E., Menéndez, J. A., Díez, M. A., Suárez, D., Montes-Morán, M. A.. Infrared Spectroscopy of Carbon Materials: A Quantum Chemical Study of Model Compounds. The Journal of Physical Chemistry B. 2003;107(26):6350-6359
99. Arasi, A. Yelil, Jeyakumari, J. Juliet Latha, Sundaresan, B., Dhanalakshmi, V., Anbarasan, R.. Ftir Spectroscopy: A Useful Tool for Structural Determination of Polyaniline and its Nanocomposites. Polymers and Polymer Composites. 2009;17(7):411-421.
100. Černý, Jaroslav. ALIPHATIC C-H BOND RESPONSES IN THE 900-700 cm^{-1}REGION OF THE FTIR SPECTRA OF COAL TARS. Fuel Science and Technology International. 1995;13(6):807-818.
101. Vinaykin, Mikhail, Benderskii, Alexander V.. Vibrational Sum-Frequency Spectrum of the Water Bend at the Air/Water Interface. The Journal of Physical Chemistry Letters. 2012;3(22):3348-3352
102. Ren, Fuzeng, Ding, Yonghui, Leng, Yang. Infrared spectroscopic characterization of carbonated apatite: A combined experimental and computational study. Journal of Biomedical Materials Research Part A. 2013;102(2):496-505.
103. Secco, Etalo A.. Spectroscopic properties of SO_4 (and OH) in different molecular and crystalline environments. I. Infrared spectra of $Cu_4(OH)_6SO_4$, $Cu_4(OH)_4OSO_4$, and $Cu_3(OH)_4SO_4$. Canadian Journal of Chemistry. 1988;66(2):329-336
104. Coates, J. P. (1996) 'The Interpretation of Infrared Spectra: Published Reference Sources', Applied Spectroscopy Reviews, 31(1–2), pp. 179–192.
105. Lizeth Katherine TN, Vendula B, Jaroslav K, Jaroslav C. Structure and Photocatalytic Properties of Ni-, Co-, Cu-, and Fe-Doped TiO(2) Aerogels. Gels. 2023;9(5).
106. Fan X, Zerebecki S, Du R, Hübner R, Marzum G, Jiang G, et al. Promoting the Electrocatalytic Performance of Noble Metal Aerogels by Ligand-Directed Modulation. Angew Chem Int Ed Engl. 2020;59(14):5706-11.
107. Ali A, Dinh CTN, Kwang-Youn C, and Oh W-C. A simple ultrasonic-synthetic route of Cu2Se-graphene-TiO2 ternary composites for carbon dioxide conversion processes. Fullerenes, Nanotubes and Carbon Nanostructures. 2018;26(12):827-36.
108. Chastain J, King Jr RC. Handbook of X-ray photoelectron spectroscopy. Perkin-Elmer Corporation. 1992;40(221):25.
109. Kozhukharov V, Machkova M, Ivanov P, Bouwmeester H, van Doorn R. Surface analysis of doped lanthanide cobalt perovskites by X-ray photoelectron spectroscopy. Journal of materials science letters. 1996;15(19):1727-9.

110. Pirker L, Višić B, Kovač J, Škapin SD, Remškar M. Synthesis and Characterization of Tungsten Suboxide W(n)O(3n-1) Nanotiles. Nanomaterials (Basel). 2021;11(8).
111. Patel, Kunjal, Solanki, G. K., Patel, K. D., Pathak, V. M.. X-ray Diffraction Analysis of Hexagonal Klockmannite CuSe Nanoparticles for Photodetectors under UV Light. The Journal of Physical Chemistry C. 2021;125(6):3517-3526.
112. Garces, Luis Javier, Hincapie, Beatriz, Zerger, Richard, Suib, Steven L.. The Effect of Temperature and Support on the Reduction of Cobalt Oxide: An in Situ X-ray Diffraction Study. The Journal of Physical Chemistry C. 2015;119(10):5484-5490.
113. Khan, G. R.. Crystallographic, structural and compositional parameters of Cu–ZnO nanocrystallites. Applied Physics A. 2020;126(4).
114. Liu, D. S., Liu, R. P., Wei, Y. H.. Influence of tungsten on microstructure and wear resistance of iron base hardfacing alloy. Materials Science and Technology. 2014;30(3):316-322.
115. Kang, Jian Xiong, Li, Xin Kuan. Thoughts on the Development of Molybdenum Beneficiation Technology. IOP Conference Series: Earth and Environmental Science. 2021;647(1):012001.
116. Bradley, A.J.. L. The crystal structures of the rhombohedral forms of selenium and tellurium. The London, Edinburgh, and Dublin Philosophical Magazine and Journal of Science. 1924;48(285):477-496.
117. Caruso, Rosario, Gambino, Grazia Laura, Scordino, Monica, Sabatino, Leonardo, Traulo, Pasqualino, Gagliano, Giacomo. Gas Chromatographic Quantitative Analysis of Methanol in Wine: Operative Conditions, Optimization and Calibration Model Choice. Natural Product Communications. 2011;6(12).
118. Thangarasu S, Bhosale M, Palanisamy G, Oh TH. Developments in Nanostructured MoS2-Decorated Reduced Graphene Oxide Composite Aerogel as an Electrocatalyst for the Hydrogen Evolution Reaction. Gels. 2024;10(9):558.
119. Rezaul Karim KM, Tarek M, Ong HR, Abdullah H, Yousuf A, Cheng CK, et al. Photoelectrocatalytic Reduction of Carbon Dioxide to Methanol Using CuFe2O4 Modified with Graphene Oxide under Visible Light Irradiation. Industrial & Engineering Chemistry Research. 2019;58(2):563-72.